

Hot New Early Dark Energy: Dark Radiation Matter Decoupling

Mathias Garny^{1,*}, Florian Niedermann^{2,†}, Henrique Rubira^{3,4,5,‡} and Martin S. Sloth^{6,§}

¹*Physik Department T31, School of Natural Sciences, Technische Universität München
James-Frank-Straße 1, D-85748 Garching, Germany*

²*Nordita, KTH Royal Institute of Technology and Stockholm University
Hannes Alfvéns väg 12, SE-106 91 Stockholm, Sweden*

³*University Observatory, Faculty of Physics, Ludwig-Maximilians-Universität, Scheinerstr. 1, D-81679 München, Germany*

⁴*Kavli Institute for Cosmology Cambridge, Madingley Road, Cambridge CB3 0HA, UK*

⁵*Centre for Theoretical Cosmology, Department of Applied Mathematics and Theoretical
Physics University of Cambridge, Wilberforce Road, Cambridge, CB3 0WA, UK*

⁶*Universe-Origins, University of Southern Denmark, Campusvej 55, 5230 Odense M, Denmark*

We present a microscopic model of the dark sector that resolves the Hubble tension within standard current datasets based on well-known fundamental principles, gauge symmetry and spontaneous symmetry breaking. It builds on the Hot New Early Dark Energy (Hot NEDE) setup, featuring a dark $SU(N)$ gauge symmetry broken to $SU(N-1)$ in a supercooled phase transition that creates a thermal bath of self-interacting dark radiation in the epoch between Big Bang Nucleosynthesis and recombination. Adding a fermion multiplet charged under the gauge symmetry provides a naturally stable component of dark matter that interacts with dark radiation. Spontaneous symmetry breaking predicts a decoupling of this interaction once the dark sector cools down, that we refer to as dark radiation matter decoupling (DRMD). We find agreement between the SH₀ES determination of H_0 as well as combined Planck 2018, Pantheon+ and DESI baryon acoustic oscillation (BAO) data at 1.4σ level, compared to a 5.7σ tension in the Λ Cold Dark Matter model. We also provide a simplified three-parameter DRMD model encoding the essential features, while the full model offers additional falsifiable predictions.

*“Such’ Er den redlichen Gewinn!
Sei Er kein schellenlauter Tor!
Es trägt Verstand und rechter Sinn
Mit wenig Kunst sich selber vor;
Und wenn’s euch ernst ist was zu sagen,
Ist’s nötig Worten nachzujagen?
Ja, eure Reden, die so blinkend sind,
In denen ihr der Menschheit Schnitzel kräuselt,
Sind unerquicklich wie der Nebelwind,
Der herbstlich durch die dürren Blätter säuselt!”
— Johann Wolfgang von Goethe*

* mathias.garny@tum.de

† florian.niedermann@su.se

‡ henrique.rubira@lmu.de

§ sloth@sdu.dk

CONTENTS

I. Introduction	2
II. Microscopic model	5
A. Overview	6
B. Hot new early dark energy	9
C. Interacting dark matter and dark radiation	11
D. One-loop dark matter mass splitting	13
E. Dark radiation matter decoupling	13
III. Evolution of perturbations	16
A. Dark matter and dark radiation perturbations	16
1. Before the phase transition ($z > z_*$)	17
2. Phase transition ($z = z_*$)	17
3. Mass-threshold effect of the Higgs ($z = z_t$)	18
4. Dark matter decoupling ($z_{\text{stop}} > z > z_{\text{dec}}$)	18
B. Dark radiation matter decoupling model	20
IV. Results	22
A. Data analysis	23
B. Results discussion	24
V. Conclusions	26
Acknowledgements	27
A. Table with MCMC results	28
B. Dark matter interacting via spontaneously broken $SU(N)$	29
1. Gauge bosons	29
2. Interacting dark matter	30
C. Computation of mass splitting	30
D. Computation of conversion cross section	32
E. Non-Abelian gauge boson interactions	33
References	34

I. INTRODUCTION

One of the main goals of particle cosmology is to use cosmological observations for probing the microphysics of the dark sector, supporting the discovery of new forces and forms of matter. In this work we argue that the observations leading to the Hubble tension allow us to approach this goal, pointing to dark sector physics governed by fundamental principles known from the visible sector to exist in Nature.

Local measurements of the expansion rate of the Universe are becoming increasingly accurate, and several different methods yield values inconsistent with those inferred indirectly from the Cosmic Microwave Background (CMB) and Baryon Acoustic Oscillation (BAO) measurements, when assuming the current standard model of cosmology, the Λ Cold Dark Matter (Λ CDM) model. Most notable, the SH₀ES measurement of local type IA supernovae (SNe) calibrated with Cepheids gives $H_0 = 73.04 \pm 1.04$ km/s/Mpc [1] (and $H_0 = 73.17 \pm 0.86$ km/s/Mpc after a recent update [2]), while a distance ladder free measurement using type II SNe finds $H_0 = 74.9 \pm 1.9$ (stat. only) km/s/Mpc [3]. In addition, there are measurements using type IA SNe calibrated via the tip of the red giant branch (TRGB) instead of Cepheids yielding $H_0 = 73.22 \pm 2.06$ km/s/Mpc [4], or 70.4 ± 2.1 km/s/Mpc in the analysis of [5]. Other independent measurements are strong lensing time-delay measurements by the TDCOSMO collaboration obtaining $H_0 = 74.8 \pm 3.5$ km/s/Mpc when combining with BAO data from the DESI galaxy survey [6], and measurements using surface brightness fluctuations, yielding $H_0 = 73.3 \pm 2.5$ km/s/Mpc [7], consistent with the other local measurements, but currently with larger error bars.

In sharp contrast with the local measurements, the predicted value of H_0 within the Λ CDM model is $H_0 = 67.36 \pm 0.54$ km/s/Mpc when using Planck 2018 CMB data [8]. Therefore, unless measurements are systematically wrong across different methods and systematics, the Λ CDM model is disfavored with very high statistical significance. In the more extreme case, using SH₀ES data, the Λ CDM model is ruled out with more than 5σ significance (for a review on the Hubble tension and its proposed solutions see [9]). Moreover, as more and more new data is being added, the Hubble tension tends to become more significant. For example, in their recent data release of ground-based CMB data, the South Pole Telescope (SPT) collaboration reports a 6.2σ tension based on SPT data alone [10], with a similar trend seen by the Atacama Cosmology Telescope (ACT) [11]. This prompts us to search for a new standard model of cosmology consistent with the data.

BAO measurements by the DESI collaboration provide an almost model-independent determination of the product $r_d \cdot H_0 = 101.54 \pm 0.73$ (100 km)/s [12], where r_d is the sound horizon at time of baryon decoupling. This means that models fitting CMB data with a larger value of H_0 than Λ CDM must do so with also a smaller value of r_d in order to keep the product $r_d \cdot H_0$ in agreement with BAO measurements. Since the sound horizon r_d only depends on the evolution of the Universe until just around recombination, models attempting to achieve agreement between CMB and the value of H_0 extracted from local measurements with only post-recombination physics generically fail badly in being consistent with BAO data. Thus, any solution to the Hubble tension, that brings consistency between CMB data, $r_d \cdot H_0$ from BAO, and H_0 from local measurements must conservatively do so by modifying pre-recombination physics or the recombination history itself [13, 14].

A simple and natural framework to address the Hubble tension by modifying pre-recombination physics is the New Early Dark Energy (NEDE) scenario [15–20]. In this setup the dark sector undergoes a fast-triggered phase transition (for recent reviews see [21] or [9], and for related work [22–25]). Within the two most studied NEDE models, the Cold and the Hot NEDE model, a strong first-order phase transition is triggered either by an ultra-light axion in vacuum in the case of Cold NEDE [15, 16, 19], or by a non-vanishing dark sector temperature in Hot NEDE [17, 18, 20]. In both cases, the vacuum energy in the false vacuum, i.e. the latent heat associated with the phase transition, becomes important in the radiation-dominated Universe before the phase transition, and is converted into a dark fluid after the phase transition. This leads to an injection of extra energy, stemming from the latent heat and/or the post-phase-transition fluid, which reduces the sound horizon and allows for a solution to the Hubble tension.

The Cold and Hot NEDE models however differ in important testable ways. In the Cold NEDE model the vacuum energy leads to an energy injection right before matter domination, which quickly decays away in a stiff NEDE fluid with equation of state $w \sim 2/3$. Since the energy density of this fluid decays away fast, the Cold NEDE phase transition has to happen relatively close to recombination, like in the axiEDE model [26] (see [27] for a review), although in axiEDE the transition happens even later between matter-radiation equality and recombination. Moreover, these models are realized by completely different microphysics, with the axiEDE model invoking an arguably exotic axion potential [28]. The Cold NEDE and axiEDE models are therefore distinct models both conceptually and also phenomenologically.

In the Hot NEDE scenario, which is the focus of this work, the latent heat of the supercooled phase transition is instead converted into dark radiation, which is not diluted away compared to ordinary radiation. It is the extra dark radiation that then leads to a decrease of the sound horizon, and the phase transition can therefore happen anywhere between Big Bang Nucleosynthesis (BBN) and recombination. In order to have a large enough effect on the sound horizon, it is important that the extra dark radiation is created *after* BBN, because otherwise it would spoil the successful prediction of light element abundances. In this respect, Hot NEDE UV-completes models of Strongly Interacting Dark Radiation (SIDR) [29–33], as it provides a way to create the large value of ΔN_{eff} assumed in SIDR models while being consistent with BBN [20]. Furthermore, the Hot NEDE model does lead to a number of new testable predictions, like a sharp feature in the matter power spectrum at small scales and a gravitational wave signal, which can be searched for using pulsar timing arrays [20]. Finally, while SIDR models cannot fully resolve the Hubble tension, we find such a solution in this work resulting from the specific microphysics of Hot NEDE.

We consider a microphysical implementation of the Hot NEDE model guided by well-known fundamental principles from the perspective of particle physics, encompassing gauge symmetries and spontaneous symmetry breaking. We assume a dark sector governed by an $SU(N)$ gauge symmetry, that is spontaneously broken to $SU(N-1)$ via the Higgs mechanism, following [20]. The associated phase transition features supercooling [34] if symmetry breaking occurs via the Coleman-Weinberg mechanism [35], and creates a thermal plasma of dark radiation with sizeable ΔN_{eff} after BBN. Furthermore, non-Abelian gauge boson self-interactions ensure that the dark radiation behaves like a fluid and does not free-stream [29, 30, 36, 37].

In this work, we extend the Hot NEDE model by including a massive Dirac fermion multiplet transforming in the fundamental representation of the $SU(N)$ gauge group of the dark sector, while being a singlet under the Standard Model gauge symmetries. Gauge and Lorentz symmetries make it stable, and thus a candidate to constitute part of dark matter. Its coupling to gauge bosons leads to an interaction between dark matter and dark radiation via a

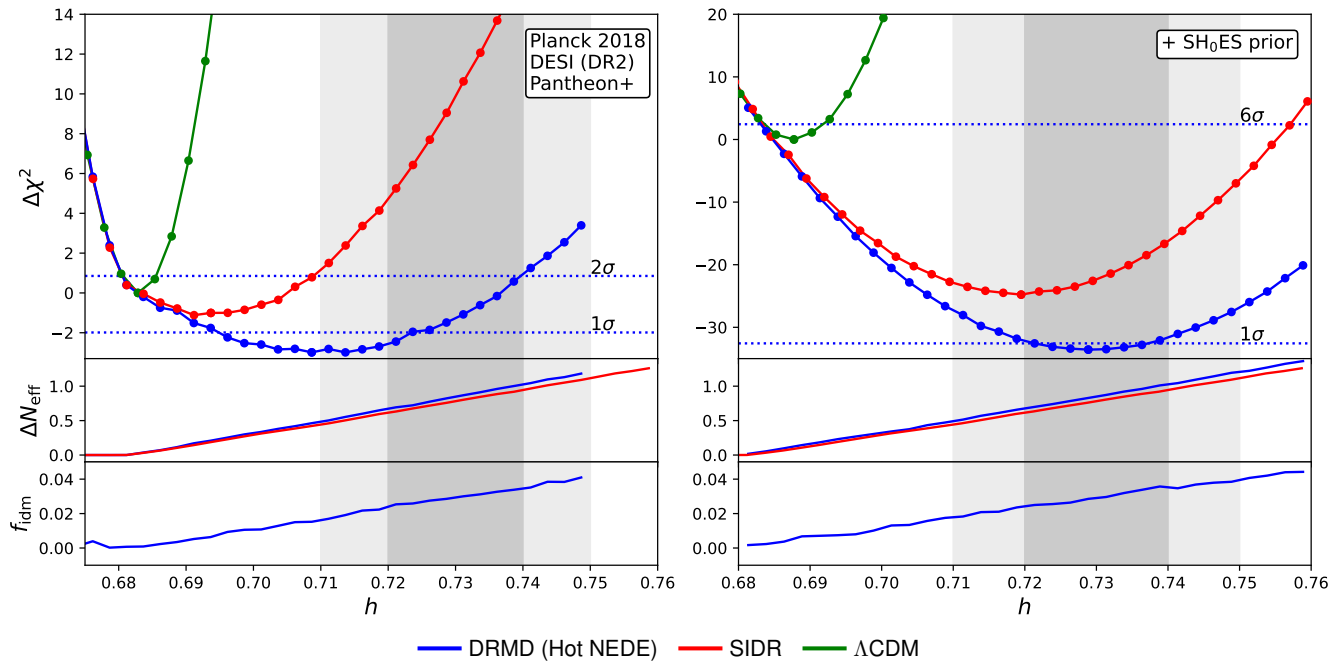


FIG. 1. Profile likelihood curves for the DRMD dark sector model, arising as a particular limit of the Hot NEDE model and proposed in this work (blue), compared to a model of self-interacting dark radiation (SIDR, red) and to Λ CDM (green). The left panel includes Planck 2018 CMB, DESI BAO (DR2), and (uncalibrated) Pantheon+ SNe data, while the right panel adds in addition the local H_0 measurement from SH₀ES in the likelihood (the 1- and 2 σ regions preferred by SH₀ES are also indicated by the gray regions in both panels for comparison). The lower panels show the model parameters of (post-BBN) ΔN_{eff} and f_{idm} (fraction of interacting dark matter). The feature of decoupling between dark radiation and dark matter within the DRMD model impacts the evolution of perturbations, making it consistent with large values of $h = H_0/(100 \text{ km s}^{-1} \text{ Mpc}^{-1})$ and ΔN_{eff} . The dark radiation is produced in a phase transition after BBN, while $\Delta N_{\text{eff}} \ll 1$ during BBN. The low- h regime corresponds to vanishing ΔN_{eff} , and the three models coincide. The DRMD model follows from a well-defined microscopic theory based on known principles, including gauge symmetry and spontaneous symmetry breaking in the dark sector.

drag force [29, 30, 36, 37] (see also [38–41]), and initially tightly couples both fluids. Spontaneous symmetry breaking induces a small mass splitting among the components of the multiplet, with the lighter one being neutral under the residual $SU(N-1)$ symmetry. An analogous property is well-known in the context of electroweak symmetry breaking for supersymmetric dark matter (see e.g. [42]). However, here it appears within the dark sector, leading to a very different phenomenology. Specifically, once the dark sector temperature drops below the mass splitting, the interactions turn off in a process we refer to as *Dark Radiation Matter Decoupling* (DRMD). Importantly, the dark radiation remains fluid-like even after this decoupling, since the self-interactions among the massless $SU(N-1)$ gauge bosons remain active. We dub this setup DRMD model. We work out and implement the evolution of perturbations in the DRMD model into a modified version of CLASS [43], and test it against Planck 2018 legacy data alongside the recently released DESI BAO (DR2) and Pantheon+ SNe data [44].

Let us briefly preview our main results. We find that our baseline data consisting of CMB, BAO and (uncalibrated) SNe is consistent with the local determination of H_0 by SH₀ES at 1.4 σ level with (effectively) only three extra free parameters compared to Λ CDM, providing a full resolution to the Hubble tension. The specific DRMD dynamics has an impact on the evolution of perturbations such that CMB and BAO data allow for a relatively large post-BBN value of ΔN_{eff} , provided that the decoupling between dark radiation and dark matter occurs at a redshift z_{dec} around matter-radiation equality, and that only a percent-level fraction f_{idm} of dark matter interacts, while the remaining part behaves as CDM (being e.g. provided by an additional field that is a singlet under $SU(N)$). Since our Bayesian analysis indicates the presence of projection effects, we also perform a profile likelihood analysis, finding consistent results regarding the ability of the model to resolve the Hubble tension (see [45] for a discussion of profile likelihood analysis in the context of EDE or [46] for Cold NEDE).

We show the profile likelihood for the DRMD model studied in this work with respect to H_0 in Fig. 1, for the case when including Planck 2018 CMB, DESI BAO (DR2), and (uncalibrated) Pantheon+ SNe data (left panel), and when combining also with the local H_0 measurement by SH₀ES implemented through a Gaussian prior on the absolute SNe magnitude (right panel). For comparison, we also show the profile likelihoods for the standard Λ CDM model as well

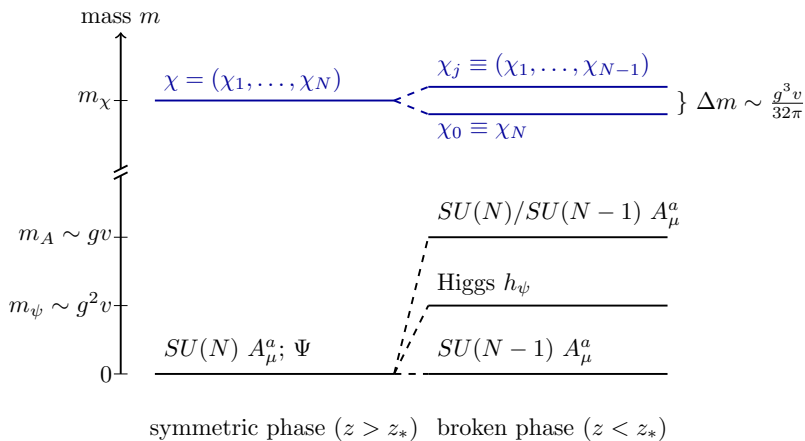


FIG. 2. Mass spectrum of the dark sector in the unbroken $SU(N)$ phase ($z > z_*$) and in the broken $SU(N-1)$ phase ($z < z_*$). The Higgs mechanism generates masses $m_A \sim gv$ of all gauge bosons A_μ^a except for those belonging to the residual $SU(N-1)$ subgroup, forming a component of self-interacting dark radiation (SIDR). The dark Higgs has a mass $m_\psi \sim g^2 v$, being characteristic for the Coleman-Weinberg mechanism. In blue, the fermion multiplet χ is shown, being (part of) dark matter. It receives a loop-induced mass splitting Δm , which makes only the neutral component χ_0 stable, while the charged χ_j states convert to the neutral one at temperatures $T_d \ll \Delta m$.

as an SIDR model (with fluid-like extra relativistic energy, assumed to be created after BBN, but no interaction with dark matter). Even when not including any local H_0 measurements in the left panel, the DRMD model prefers large values in a wide range $h \simeq 0.69 - 0.73$, featuring a flat $\Delta\chi^2$ such that $h = 0.73$ is allowed at the $\sim 1.5\sigma$ level, in stark contrast to the SIDR model. The right panel shows the resulting significant improvement $\Delta\chi^2 \simeq -33$ when including the local SH₀ES measurement for DRMD. The lower panels depict the model parameters ΔN_{eff} and f_{idm} .

We note that the specific aspect of an interaction rate between dark radiation and dark matter components that becomes suppressed at some point during cosmological evolution has been considered in completely different microphysical setups, such as dark recombination in atomic dark matter [47–51], due to the mass of the particle mediating the interaction [38, 39, 52], or decay of the latter [53]. However, these setups differ in their cosmological evolution from the Hot NEDE model, as well as in the details of how the interaction becomes suppressed, and whether the dark radiation remains fluid-like or starts to free-stream, which turn out to be relevant for the ability to address the Hubble tension. Interactions between dark matter and dark radiation described by a drag force have also been discussed in e.g. [29, 30, 36–40, 52–59].

This work is structured as follows: In Sec. II, we first provide an overview over the microscopic model and its cosmological evolution, with a subsequent detailed discussion including a review of the phase transition dynamics following [20] as well as the novel aspects related to the dark matter multiplet. The evolution of perturbations is discussed in Sec. III, first for the full model and then for a simplified setup capturing only the essential DRMD features, that we employ in our data analysis. In Sec. IV we present our results and conclude in Sec. V. The appendices contain a table with further information on our results (Appendix A) as well as computational details.

II. MICROSCOPIC MODEL

In this section we discuss the microphysical model. We assume a dark sector that is sequestered from the visible sector, but governed by known fundamental principles, i.e. gauge symmetry complemented by the Higgs mechanism. Taking these as an inspiration, we consider a dark $SU(N)$ gauge symmetry, that is spontaneously broken to $SU(N-1)$ by a dark Higgs field Ψ [20]. Moreover, in this work, we incorporate also a fermionic multiplet χ charged under $SU(N)$ that describes (part of) dark matter (while the remaining part is assumed to be standard CDM). Before a more detailed discussion, we provide an overview of the main features and the resulting cosmological evolution.

A. Overview

The Lagrangian describing the microphysics of the dark sector is largely dictated by the assumed gauge symmetry, and given by the canonical form

$$\mathcal{L} = \bar{\chi}(i\gamma^\mu D_\mu - m_\chi)\chi + |D\Psi|^2 - V_{\text{cl}}(|\Psi|^2) - \frac{1}{4}F_{\mu\nu}^a F_a^{\mu\nu}, \quad (1)$$

with $F_a^{\mu\nu}$ the field strength tensor of the dark gauge fields A_a^μ , associated to the generators τ_a of $SU(N)$. We assume both the dark Higgs field $\Psi = (\Psi_1, \dots, \Psi_N)$ and the dark matter multiplet $\chi = (\chi_1, \dots, \chi_N)$ to transform under the fundamental representation of $SU(N)$, such that their gauge interaction is determined by the usual covariant derivative $D^\mu = \partial^\mu - igA_a^\mu \tau_a$ with gauge coupling g assumed to be perturbatively small, i.e. $g^2/(4\pi) \ll 1$. The potential V_{cl} is given by the standard form, see (4) below, and gives rise to spontaneous symmetry breaking $SU(N) \rightarrow SU(N-1)$ via the Higgs mechanism, with vacuum expectation value (VEV) that can without loss of generality be parameterized as $\langle \Psi \rangle = (0, \dots, 0, v/\sqrt{2})$. For simplicity we assume χ to be a Dirac fermion, allowing for a Dirac mass term but precluding a Yukawa interaction with Ψ . The relevant fundamental parameters are thus the VEV v , the gauge coupling g and the dark matter mass scale m_χ . Following [20] we assume the Higgs potential to be (close to) classically scale-invariant, such that v is generated by dimensional transmutation via the Coleman-Weinberg mechanism [35] (being parametrically the scale at which the running quartic Higgs coupling $\lambda(v)$ is of the order of g^4 , thus trading λ for v as model parameter). The dimensionful scales are therefore ‘protected’ by chiral and scale symmetries, respectively.

The mass spectrum in the symmetric and the broken phase is illustrated in Fig. 2. In the latter, the gauge bosons related to the residual $SU(N-1)$ subgroup remain massless, while the other ones acquire a mass of order $m_A \sim gv$ and famously absorb all (Goldstone) components of the Higgs multiplet Ψ except for a single degree of freedom, being the (dark) Higgs boson. The Coleman-Weinberg mechanism requires its mass to be of order $m_\psi \sim g^2 v$. Finally, χ splits into the two subsets $\chi_0 \equiv \chi_N$ and $\chi_j \equiv (\chi_1, \dots, \chi_{N-1})$, being neutral and charged under the residual $SU(N-1)$, respectively. Radiative corrections induce a (small) mass splitting $\Delta m \sim g^3 v/(32\pi)$, making χ_0 slightly lighter. Notably, the splitting Δm is independent of m_χ for $m_\chi \gg m_A$ [42], which we assume in the following. Apart from this, the ordering of mass scales generated via spontaneous symmetry breaking,

$$m_A \sim gv \gg m_\psi \sim g^2 v \gg \Delta m \sim g^3 v/(32\pi), \quad (2)$$

is a direct consequence of the microphysical setup (with viable values of the gauge coupling being $g \sim \mathcal{O}(0.1)$). This mass hierarchy has a decisive impact on its cosmological evolution, with specific dynamics linked to the redshifts at which the temperature of the dark sector drops below each of those mass scales.

An outline of the cosmological evolution, as discussed in detail below, is as follows:

- The (secluded) dark sector is initially populated in the Early Universe, and is then subsequently completely decoupled from the visible sector. While the precise mechanism is irrelevant here, a suitable possibility is freeze-in [60] (e.g. minimally via gravitational interactions [61]). Dark gauge interactions establish thermal equilibrium in the dark sector, at some initial temperature $T_d \ll T_{\text{vis}}$ that we assume to be (much) smaller than the one in the visible sector¹.
- Once T_d drops below m_χ the abundance of χ remains fixed, and provides a constant fraction $f_\chi \equiv f_{\text{idm}}$ of the total dark matter density. The details of this dynamics is left unspecified in this work, and we treat f_χ as a free parameter. A generic scenario is freeze-out of χ within the dark sector into dark gauge and Higgs bosons, featuring an interesting but also rather complex dynamics [63–65]. Subsequently, the dark sector consists of a SIDR component formed by the gauge and Higgs bosons, and a non-relativistic interacting dark matter (IDM) component, given by the χ multiplet, that interacts with the SIDR via gauge interactions.
- During the BBN epoch, $z \sim 10^9$, the low initial dark sector temperature leads to a negligible relativistic energy density, denoted by $\Delta N_{\text{BBN}} \ll 1$. Its precise value is irrelevant for the subsequent evolution, but ensures that standard BBN predictions are not spoiled by the dark sector.
- At some redshift $z = z_*$, after the BBN epoch, the dark sector undergoes a first-order phase transition $SU(N) \rightarrow SU(N-1)$. As is well-known, the Coleman-Weinberg setup leads to strong supercooling, with a sizeable vacuum energy being released into the dark sector [34]. The value of z_* is set by the small deviation from scale-invariance

¹ In the self-interacting Planckian interacting dark matter (PIDM) scenario one naturally has $T_d \sim 10^{-3} T_{\text{vis}}$ [62].

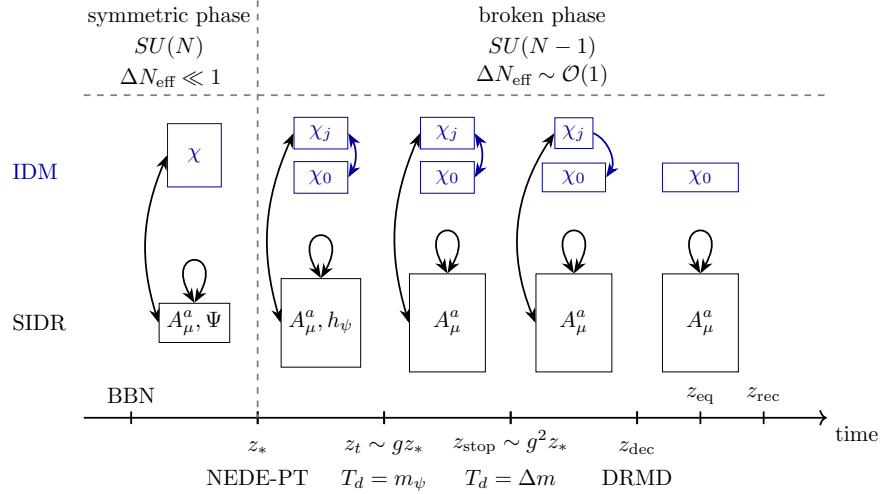


FIG. 3. Schematic illustration of the cosmological evolution of the dark sector, consisting of self-interacting dark radiation (SIDR) and interacting dark matter (IDM). During BBN the dark sector contribution to the total radiation energy is negligible. The vacuum energy released in the supercooled NEDE phase transition (NEDE-PT) at $z = z_*$ reheats the dark sector, and leads to a splitting between charged (χ_j) and neutral (χ_0) IDM components. At $z = z_t$ the Higgs drops out of the SIDR plasma, and at $z = z_{\text{stop}}$ the occupation of χ_j becomes Boltzmann suppressed relative to χ_0 . This leads to a termination of the tight coupling between IDM and SIDR at $z = z_{\text{dec}}$ (dark radiation matter decoupling, DRMD), resolving the Hubble tension if z_{dec} occurs around matter-radiation equality (z_{eq}), slightly before recombination (z_{rec}). For comparison with the stepped SIDR model, we refer to Fig. 1 of [53]. Black arrows indicate energy/momentum exchange in elastic processes such as e.g. $\chi_j A_\mu^a \leftrightarrow \chi_j A_\mu^a$, and blue arrows additionally conversions among χ_j and χ_0 states.

in the Higgs potential, related to the quadratic term. The latter only affects z_* , being therefore effectively a free model parameter. The phase transition is assumed to be after BBN but sufficiently long before recombination, roughly $10^4 \ll z_* \lesssim 10^9$.

- The latent heat increases the entropy of the dark sector and reheats it to a temperature $T_d \sim gv$ after the phase transition, creating a sizeable contribution to the radiation energy,

$$\Delta N_{\text{eff}} \equiv \Delta N_{\text{NEDE}} \sim \left(\frac{gv}{85 \text{ keV}} \right)^4 \left(\frac{10^8}{1+z_*} \right)^4 \quad (\text{for } N=3), \quad (3)$$

carried by the massless $SU(N-1)$ gauge bosons and the Higgs boson [20]. This energy injection is primarily responsible for lowering the sound horizon r_d , and the resulting order of magnitude $\Delta N_{\text{NEDE}} \sim \mathcal{O}(1)$ to address the Hubble tension sets the overall phase transition scale gv . Since $m_\chi \gg gv$ we assume that the χ abundance is not affected by the phase transition, even though a more detailed study of this point would be interesting (see e.g. [66]). The χ_0 component becomes slightly lighter than χ_j due to the mass splitting Δm . However, since $T_d \sim gv \gg \Delta m$, all components of χ are equally populated at this time, as dictated by equipartition.

- Gauge interactions ensure that conversions among the χ_0 and χ_j components are in equilibrium. The charged states efficiently Compton scatter $\chi_j A_\mu^a \leftrightarrow \chi_j A_\mu^a$ off the massless gauge bosons, leading to a drag force that is enhanced due to the non-Abelian interaction [29, 37, 39, 67] (as compared to the analogous baryon-photon scattering process). Overall, this creates a single, tightly coupled fluid in the dark sector with common sound velocity $c_s \ll 1/\sqrt{3}$.
- At redshift $z = z_t \sim gz_*$ the temperature T_d drops below $m_\psi \sim g^2 v$ and the Higgs becomes non-relativistic. It drops out of the plasma and slightly increases ΔN_{eff} (while preserving entropy) due to the mass-threshold effect [33], leading to a slight further increase to the final value ΔN_{IR} [20]. While this ‘second step’ is a prediction of the model, we find its phenomenological impact to be small. Moreover, the size of this second step vanishes in the large- N limit of the dark $SU(N)$.
- At $z = z_{\text{stop}} \sim g^2 z_*$, the temperature T_d becomes smaller than the mass splitting Δm . Subsequently the heavier charged components χ_j of the dark matter multiplet become Boltzmann suppressed relative to χ_0 ,

$n_{\chi_j}/n_{\chi_0} \sim e^{-\Delta m/T_d} = e^{-z_{\text{stop}}/z}$. Nevertheless, the drag force due to gauge interaction still maintains tight coupling, but the effective rate quickly drops since the massless gauge bosons effectively Compton scatter only off the charged χ_j states.

- At $z = z_{\text{dec}} \sim z_{\text{stop}}/30$ tight coupling breaks down. Afterwards, the massless gauge bosons form a fluid component of self-interacting dark radiation (i.e. with $c_s = 1/\sqrt{3}$ but no anisotropic stress), and the dark matter (now being predominantly in the neutral state χ_0) behaves as distinct matter component approaching CDM behaviour. This is the process of DRMD which we find is crucial to resolve the Hubble tension if z_{dec} occurs somewhat before recombination. For the scales we consider, the ratio $z_{\text{dec}}/z_{\text{stop}}$ is the only place where m_χ enters, with only a logarithmic sensitivity, see (31).

A sketch of the cosmological history is shown in Fig. 3. The essential DRMD dynamics is captured by the last two items, which are the focus of the effective DRMD model introduced in Sec. III B. It is applicable for CMB observables in the limit in which the phase transition ($z = z_*$) occurs after BBN but well before modes measured in the CMB angular power spectra enter the horizon, roughly $10^6 \lesssim z_* \lesssim 10^9$, and if the ‘second step’ at $z = z_t$ is sufficiently small (large- N limit of $SU(N)$). Nevertheless, we note that the full model, including the phase transition, is relevant for predicting features in the matter power spectrum at (small) scales entering the horizon at $\sim z_*$, for a potential gravitational wave signal either from the scalar field [68–70] or from fluid sound waves [71–74] which is specially compelling in face of the recent PTA results [75, 76], and for consistency with BBN [20]. A further potential signature of the phase transition are traces of stochasticity from the finite size of bubbles when they percolate [16, 77]. A naive comparison to constraints derived assuming this effect on top of Λ CDM perturbations suggests that they are easily satisfied for phase transitions that occur either sufficiently early ($z_* \gtrsim 10^6 - 10^7$) or on a time-scale (denoted conventionally by $1/\beta$) that is a sufficiently small fraction of the Hubble time H_* , roughly $\beta/H_* \gtrsim \mathcal{O}(10 - 100)$ for $z_* \lesssim 10^6$.

From a broader perspective, we note formal similarities of the DRMD mechanism to the breakdown of tight coupling among e^- , p and photons in the visible sector due to recombination, in the sense that the abundance of electrically charged states (i.e. e^- and ionized hydrogen) becomes small below a certain redshift, in analogy to the χ_j abundance at $z < z_{\text{stop}}$ as considered here. However, in stark contrast to the photons within the visible sector, the dark radiation does *not* start to free-stream after decoupling from the IDM component at $z > z_{\text{dec}}$, but rather remains described by a SIDR fluid due to its non-Abelian self-interactions (meaning specifically that its sound velocity increases due to DRMD, but anisotropic stress and higher multipoles remain small). Moreover, the microphysics and resulting processes and rates are very different. Nevertheless, keeping the formal analogy to certain aspects of recombination in mind, it would be interesting to investigate further details of the DRMD process. We refer to Sec. II E for further discussion of this point.

Once more, we emphasize the conceptual simplicity of the model considered in this work, with a dark $SU(N)$ gauge symmetry and fermions coupled to this dark sector. The model contains four micro-physical parameters: g, v (or alternatively λ), the effective Higgs mass μ_{eff} and m_χ , the last being effectively irrelevant, together with the discrete gauge group parameter N . Those are complemented with f_{idm} and the redshift of the phase transition z_* (or alternatively ΔN_{eff}).² As we describe later and already mentioned, effectively only three parameters describe the macrophysics of the DRMD fluid relevant to the Hubble tension, being ΔN_{eff} , f_{idm} and z_{dec} . We also refer to Table I of [20] for the typical values of parameters related to the phase transition.

We note that in [53] a model exhibiting a similar DRMD mechanism was considered (dubbed strongly interacting stepped radiation, see also [52]). However, due to the different microphysics, in that scenario a sizeable ‘step’ in ΔN_{eff} occurs coincidentally with an onset of Boltzmann suppression of the drag rate between IDM and SIDR. We identify this distinct feature as a cause for the finding from [53] regarding the moderate success of that setup in addressing the Hubble tension, in contrast to the model discussed in this work, where ΔN_{eff} is constant during the DRMD dynamics.³ Another scenario for which an IDM component stops interacting with a dark radiation component is ‘atomic dark matter’ [47–51], featuring a dark recombination process. However, in that setup the dark radiation starts to free-stream after dark recombination, similarly as for photons, making this scenario rather different from the one considered here at the level of perturbations. Nevertheless, we note that the mechanism of DRMD as predicted by the $SU(N)$ dark sector could still be realized in different microphysical setups than the one we consider here, providing avenues for future investigation.

² Also related to the NEDE fraction in [20].

³ Since the microscopic model considered in [53] requires the presence of a step in ΔN_{eff} at the same redshift for which exponential suppression of IDM-DR interaction sets in, the authors did not investigate the limiting case for which such a step is absent in detail. Nevertheless, in Fig. 13 of [53] a scenario with variable stepsize is analyzed, reporting a preference towards small values and improved χ^2 . However, those results combine CMB with SH₀ES and also S₈ data, such that a direct comparison to our work is difficult. This also means that no quantification of the (potential relaxation of the) Hubble tension for small (or variable) step size is possible from the results shown in Fig. 13 of [53].

Let us now turn to a detailed discussion of the evolution outlined above. We first review the phase transition dynamics in Sec. IIB following [20], and turn to the novel aspects from incorporating the dark matter multiplet χ in Sec. IIC, proceeding to the impact of the mass splitting in Sec. IID and the DRMD effect in Sec. IIE.

B. Hot new early dark energy

Before introducing a fermion dark matter multiplet, we first review the base Hot NEDE model introduced in [20] (building on the earlier works [17, 18]). Concretely, we consider the spontaneous breaking of a dark $SU(N)$ gauge group down to $SU(N-1)$, induced by non-zero dark temperature corrections to the NEDE Higgs potential

$$V_{\text{cl}}(|\Psi|^2) = -\mu^2|\Psi|^2 + \lambda|\Psi|^4 + V_0, \quad (4)$$

where μ is a mass scale, λ is the dimensionless quartic coupling, and V_0 an additive constant.

At non-zero dark temperature T_d , this potential will receive two types of corrections, one-loop zero-temperature quantum corrections and finite temperature thermal corrections. Accounting for both of them, the effective potential can be written as

$$V(\psi; T_d) = V_0 - \frac{\mu_{\text{eff}}^2}{2} \psi^2 \left(1 - \frac{\psi^2}{2v^2}\right) + B\psi^4 \left(\ln \frac{\psi^2}{v^2} - \frac{1}{2}\right) + \Delta V_{\text{thermal}}(\psi; T_d), \quad (5)$$

where $\psi = \sqrt{2}|\Psi|$, μ_{eff} is the effective one-loop mass providing an explicit breaking of the classical conformal symmetry, and v is the scale generated by dimensional transmutation at zero temperature by the Coleman-Weinberg mechanism [35] in the limit $\mu_{\text{eff}} \rightarrow 0$. The B parameter is given by $B = c_1 n_A (g/2)^4 / (64\pi^2)$, where g is the gauge coupling, $n_A = 3(2N-1)$ is the number of gauge bosons degrees of freedom living in the coset $SU(N)/SU(N-1)$ and acquiring a mass in the phase transition, and c_1 is a constant of order unity, which depends on N (e.g. $c_1 = 52/45$ for $N = 3$). Finally, the last term denotes the thermal corrections, which we discuss below.

The phenomenologically interesting regime in the context of the Hubble tension is when the false vacuum energy becomes cosmologically relevant after a period of strong supercooling, leading to a significant energy injection when the latent heat is released. This requires that the gauge boson mass $m_A = gv/2$ is heavy compared to the Higgs mass [34], as occurs naturally in the Coleman-Weinberg regime [35],

$$m_\psi^2 = 2\mu_{\text{eff}}^2 + 8Bv^2 \ll m_A^2 \sim g^2v^2, \quad (6)$$

and $m_A \gg T_d^*$, where T_d^* is the dark sector temperature right before the phase transition. For typical values of those parameters, see Table I of [20]. The soft breaking term μ_{eff} allows us to control the amount of supercooling prior to the phase transition. In particular, as we will show below, in order to have some amount of supercooling, the effective mass must remain small $\mu_{\text{eff}}^2 \lesssim v^2 g^4 \sim m_\psi^2$, which is a technically natural choice due to the enhanced symmetry in the limit $\mu_{\text{eff}} \rightarrow 0$.

At high temperatures, the $SU(N)$ symmetry is restored by thermal corrections, while at low temperatures, when thermal corrections can be ignored, the NEDE scalar Ψ acquires a vacuum expectation value, breaking $SU(N)$ down to $SU(N-1)$. After symmetry breaking, i.e., for temperatures far below a critical temperature T_c since we consider supercooling, it can be written in the form

$$\Psi = e^{2i\pi^a \tau^a / v} \begin{pmatrix} 0 \\ \dots \\ \frac{v}{\sqrt{2}} + \frac{h_\psi}{\sqrt{2}} \end{pmatrix}. \quad (7)$$

Here we denoted the physical mode of the dark Higgs field after the phase transition by h_ψ , and we have introduced the Goldstone fields related to the $2N-1$ broken generators by π^a . These Goldstone modes are absorbed by the gauge bosons acquiring mass in the unitary gauge.

This process can be understood in greater detail by considering the ψ -dependence of the thermal corrections $\Delta V_{\text{thermal}}(\psi; T_d)$. For $\psi \ll T_d/g$, the leading thermal correction to the NEDE scalar potential is

$$\Delta V_{\text{thermal}}(\psi; T_d) \rightarrow \frac{c_0 n_A}{24} g^2 T_d^2 \psi^2, \quad (8)$$

where c_0 is a constant of order unity which depends on N ($c_0 = 4/15$ for $N = 3$) [20]. In particular, at sufficiently high temperatures, this term creates a thermal barrier that keeps the field in the symmetric phase at $\psi = 0$. On the other hand, for large field values $\psi \gg T_d/g$, the thermal corrections to the potential are exponentially suppressed

(assuming the condition in (6) holds). This suppression becomes relevant as the dark sector temperature drops with the expansion of the Universe. Concretely, a second minimum at $\psi = v(T_d)$ appears and becomes degenerate with the symmetric minimum at the critical temperature $T_c \sim gv$ (for $\mu_{\text{eff}}^2 \lesssim v^2 g^4$). As the temperature drops further, we are entering the supercooling regime where the thermal correction in (8) keeps the field trapped at $\psi = 0$ despite the presence of a lower minimum. By comparing the tachyonic mass term in (5), $-\mu_{\text{eff}} \psi^2/2$, with the positive thermal mass in (8), we find that the barrier eventually vanishes at

$$T_b^2 = \frac{12\mu_{\text{eff}}^2}{c_0 n_A g^2} = \frac{\gamma}{\pi} g^2 v^2, \quad (9)$$

where the supercooling parameter γ is defined as [18]

$$\gamma \equiv \frac{12\pi}{c_0 n_A} \frac{\mu_{\text{eff}}^2}{v^2 g^4}. \quad (10)$$

If γ is less than one⁴, the phase transition occurs by bubbles of the true vacuum nucleating⁵ in the supercooled regime shortly before the barrier vanishes

$$T_d^* \simeq T_b = \sqrt{\frac{\gamma}{\pi}} gv \sim \sqrt{\gamma} T_c. \quad (11)$$

Quantities with a star are evaluated at bubble nucleation time. In particular, for $\gamma \ll 1$, the phase transition occurs at a temperature much below the critical temperature, $T_d^* \ll T_c$, meaning in the strongly supercooled regime where the potential energy difference between the two minima is significant at the time of the phase transition. The released latent heat is given more precisely by

$$\Delta V_* \simeq [V(\psi = v) - V(\psi = 0)]|_{T_d=0} = T_b^4 \frac{(3c_1 + 128\pi c_0 \gamma) n_A}{6144 \gamma^2}. \quad (12)$$

In the following we assume a sufficiently strong gauge coupling [20]

$$g \gtrsim 0.02, \quad (13)$$

such that the phase transition leads to an almost instantaneous reheating of the dark sector, which proceeds through the loop-induced decay of the NEDE Higgs condensate into massless gauge bosons, $\psi \rightarrow A + A$, and the subsequent thermalization via gauge bosons self-interactions $A + A \leftrightarrow A + A$ and (inverse) decays $A + A \leftrightarrow \psi$ (see [20]).

Since the latent heat is released into radiation, a mix of relativistic gauge and the NEDE Higgs bosons, this causes a step-like increase in the effective number of relativistic degrees of freedom N_{eff} . The dark sector contribution to N_{eff} can be quantified in terms of the temperature ratio $\xi = T_d/T_{\text{vis}}$ as

$$\Delta N_{\text{eff}} = \frac{4}{7} \left(\frac{11}{4} \right)^{4/3} g_{\text{rel,d}} \xi^4, \quad (14)$$

where $g_{\text{rel,d}}$ and $g_{\text{rel,vis}}$ are the numbers of relativistic bosonic degrees of freedom in the dark and visible sector, respectively. Note that ΔN_{eff} can be fixed in terms of g , v and z_* according to (3). Using that the dark sector temperature at the time of the phase transition is given by (11), we can compute the small contribution to N_{eff} *before* the phase transition as

$$\Delta N_{\text{BBN}} \simeq 0.055 \frac{\frac{N^2+N-1}{2N-1}}{11/5} \left(\frac{\gamma}{0.01} \right)^2 \frac{52/45}{c_1} \frac{\Delta V_*/\rho_{\text{tot}}(T_d^*)}{0.08}. \quad (15)$$

Immediately *after* the phase transition, during the fast coalescence and reheating stage, the latent heat is converted into radiation. This leads to a jump in N_{eff}

$$\Delta N_{\text{BBN}} \rightarrow \Delta N_{\text{NEDE}} = \frac{5(3c_1 + 128c_0\pi\gamma)n_A}{1024\pi^2 g_{\text{rel,d}}^* \gamma^2} \Delta N_{\text{BBN}}, \quad (16)$$

⁴ We still assume that γ is not exponentially small and in fact larger than $\sim 1/(g^2) \exp(-1/g^3)$. If this condition fails, the effective mass can be neglected and tunneling occurs as it would in the pure Coleman-Weinberg case, questioning whether the percolation condition could be satisfied.

⁵ We assume the bubble size to be small compared to the horizon scales at nucleation, such that the CMB is not affected by curvature fluctuations created during the phase transition [16, 77]. As argued in [18, 20], this can be achieved with very mild restrictions on the gauge coupling or a sufficiently early phase transition that occurs before modes observable in the CMB enter the horizon.

where $g_{\text{rel,d}}^*$ is the effective number of relativistic dark sector species just before the transition time (see Table II of [20]). We see that a strongly supercooled Hot NEDE phase transition with $\gamma \ll 1$ leads to a strong reheating of the dark sector after BBN and a sharp step-like increase in ΔN_{eff} . Combining (15) and (16), the parameter γ drops out and we recover (3) (up to $\mathcal{O}(1)$ numerical prefactors).

Due to the gauge interactions, the dark radiation is tightly-coupled with itself, which leads to a fluid-like behavior with vanishing higher moments, providing a natural realization of the SIDR scenario. Once the dark temperature drops below the mass m_ψ of the NEDE boson, it becomes non-relativistic and decays into $2[(N-1)^2 - 1]$ degrees of freedom associated with the massless gauge bosons. This corresponds to a second smaller reheating of the dark sector, causing another increase in N_{eff} (while conserving entropy, in contrast to the phase transition). This second step occurs at a redshift z_t implicitly defined through $T_d(z_t) = m_\psi \sim g^2 v$. We thus have

$$\frac{1+z_*}{1+z_t} = \frac{T_d^{*,\text{after}}}{m_\psi} \simeq \frac{c_o}{g}. \quad (17)$$

where $T_d^{*,\text{after}} \sim \mathcal{O}(gv)$ is the temperature after the dark sector reheating at $z = z_*$. The last equality assumed $\gamma \ll 1$ and introduced an N -dependent factor that evaluates to $c_o = (5/91)^{1/4} \sqrt{6} \simeq 1.19$ for $N = 3$ [20]. Using that the total entropy of the fluid is conserved, we derive the step size as

$$\Delta N_{\text{NEDE}} \rightarrow \Delta N_{\text{IR}} = \Delta N_{\text{NEDE}} (1+r_g)^{1/3}, \quad (18)$$

where $r_g = (2N(N-2))^{-1}$ is the relative change in the number of relativistic degrees of freedom. Although being a prediction of our model, this second step led only to a minor improvement of the fits to the observables [20].

SIDR models have been considered as proposed solutions to the Hubble tension for a while. However, it is well known that they can only provide a small alleviation of the Hubble tension, and even then, they require a too high $\Delta N_{\text{eff}} \simeq 0.5$, which is excluded by BBN. This is where the Hot NEDE model steps in. The first step in N_{eff} after BBN in (16) provides the large initial value of $\Delta N_{\text{eff}} \simeq 0.5$ without being in conflict with BBN constraints. In [33], an SIDR model with a step in N_{eff} similar to the second step in (18) was proposed. However, the model of [33] does not feature a first step and is therefore ruled out by BBN unless UV completed with a first step as in Hot NEDE⁶. Also note that the model considered in this work is qualitatively different than scenarios for which the ΔN_{eff} step generates a relative feature between the large and small-scale multipoles of the CMB [33, 53, 83]. In our case, the first ΔN_{eff} step (16) acts to reheat the dark radiation sector way before recombination and after BBN (reminding that the second small step (18) has only very little impact).

In this way, Hot NEDE, featuring the two-step sequence, $\Delta N_{\text{BBN}} \rightarrow \Delta N_{\text{NEDE}} \rightarrow \Delta N_{\text{IR}}$, can be viewed as a UV completion of the (stepped) SIDR model. As we will see below, when we add a fermion dark matter multiplet to the model, Hot NEDE also features a decoupling between dark radiation and dark matter, which leads to a full resolution of the Hubble tension. This emphasizes the importance and power of detailed realistic model building.

C. Interacting dark matter and dark radiation

In this work, we consider an extension of the Hot NEDE model, adding also a fermion χ charged under $SU(N)$, similarly as in the visible sector. Gauge and Lorentz symmetries automatically ensure stability (similar as for the electron), making χ a candidate to compose part of dark matter. For concreteness, we assume that a fraction⁷ f_χ of dark matter is a Dirac fermion χ with mass m_χ that transforms in the fundamental representation. Its Lagrangian reads

$$\mathcal{L} = \bar{\chi}(i\gamma^\mu D_\mu - m_\chi)\chi, \quad (19)$$

where $\chi = (\chi_1, \dots, \chi_N)$ labels the N Dirac spinor components of the gauge multiplet, and with γ^μ being the Dirac matrices. We further assume that m_χ is far above the dark sector temperature before and after the phase transition, such that it is sufficiently non-relativistic in the epoch between BBN and recombination, with conserved total number density when adding up the abundances of all N components.

The gauge interaction of dark matter has several consequences. Most importantly, it implies that dark matter interacts with the dark radiation via Compton scattering. This leads to a momentum exchange, and a corresponding

⁶ An alternative mechanism for generating the large initial N_{eff} through thermalization with neutrinos was considered in [78], and further mechanisms have been discussed, e.g. via domain wall [79] or particle decays [80, 81], see also [82] for a recent analysis.

⁷ In the phenomenological sections, we will use the conventional notation $f_{\text{dm}} = f_\chi$.

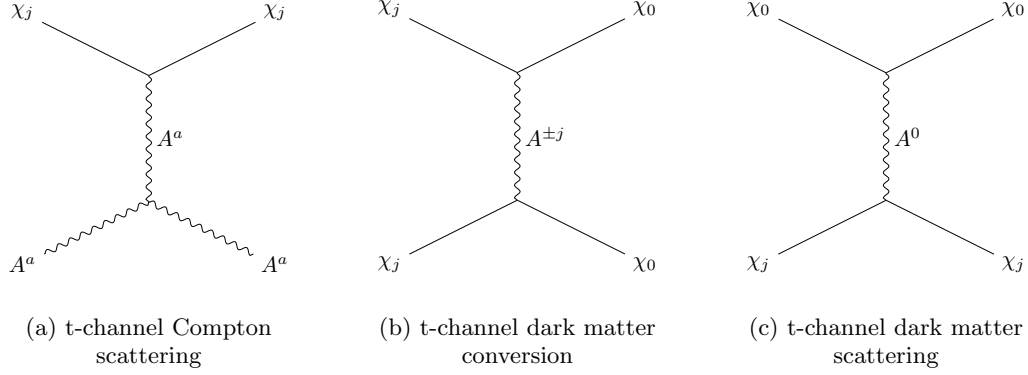


FIG. 4. Dominant processes relevant for dark matter–dark radiation decoupling. (a) t-channel Compton scattering within the $SU(N-1)$ gauge sector maintains tight coupling between dark matter and dark radiation as long as the associated drag rate satisfies $\Gamma_{\text{drag}} \gg H$; (b) t-channel conversion is relevant for chemical equilibrium between light and heavy dark matter states if the corresponding conversion rate satisfies $\Gamma_{\text{conv}} \gg H$; (c) t-channel scattering between charged and neutral dark matter states establish kinetic equilibrium within the χ sector.

change in the dark matter perturbations. More precisely, the interaction rate of dark matter with dark radiation is determined by the dark Compton scattering process of χ with massless gauge bosons, $\chi A \rightarrow \chi A$. The non-Abelian gauge bosons self-interaction enhances the scattering cross section significantly by allowing for a t -channel contribution, that is absent in the Abelian case [29, 30, 37, 67]. Similarly to baryon-photon interactions, this interaction leads to a drag force between the interacting dark matter and dark radiation components [29, 39, 40]. If the interaction rate is large enough (compared to the Hubble rate), both approach the tightly coupled limit [30, 40].

While the gauge interactions of the dark matter multiplet are discussed in more detail in Appendix B, we summarize the key results here for convenience. Before the phase transition, in the unbroken $SU(N)$ phase, we have $N^2 - 1$ massless gauge bosons A_μ^A transforming in the adjoint representation of $SU(N)$ with $A = 1, \dots, N^2 - 1$. After the phase transition, when $SU(N)$ has been spontaneously broken to $SU(N-1)$, we have the $(N-1)^2 - 1$ massless gauge bosons A_μ^a transforming in the adjoint of $SU(N-1)$ with $a = 1, \dots, (N-1)^2 - 1$, and in addition $N-1$ massive (and non-relativistic) gauge boson pairs $A_\mu^{\pm j}$ with $j = 1, \dots, N-1$ and mass $m_{A^\pm} = gv/2$ transforming in the fundamental representation of $SU(N-1)$, as well as a massive gauge boson A_μ^0 with mass $m_{A_\mu^0} = gv\sqrt{(N-1)/(2N)}$ being a singlet under $SU(N-1)$. Moreover, we distinguish between the $N-1$ components $\chi_j = (\chi_1, \dots, \chi_{N-1})$ that transform under the remaining unbroken $SU(N-1)$ and the neutral component $\chi_0 \equiv \chi_N$.

After symmetry breaking, only the massless $SU(N-1)$ gauge bosons A_μ^a remain in the dark radiation bath (alongside the relativistic Higgs h_ψ). The singlet state χ_0 of the dark matter multiplet does not feature direct renormalizable couplings to them. While a coupling of χ_0 to the A^0 exists, the latter does not couple to a pair of massless gauge bosons, precluding also a t -channel scattering of χ_0 with massless gauge bosons via A^0 exchange. Thus, at leading order in the gauge coupling, only the χ_j states of the dark matter multiplet have an interaction $\chi_j A^a \rightarrow \chi_j A^a$ with the massless gauge bosons. It results from the $SU(N-1)$ gauge interactions that dominantly proceed via the t -channel diagram in Fig. 4(a), plus an additional t -channel diagram with an A^0 . The latter, due to its mass, is however relatively suppressed at low temperatures $T \ll m_{A^0}$ after the phase transition. The reason is that the t -channel propagator is enhanced for massless gauge bosons, for which it is regulated by the thermal mass of order gT , which is much smaller than the gauge boson mass $m_{A^0} \sim gv$. Altogether, this means the interaction rate of the charged dark matter states, χ_j , with the dark radiation bath coincides with that computed for an unbroken $SU(N-1)$ gauge theory. The rate entering the drag force is thus given by [29, 30, 37, 67]

$$\Gamma_{\chi_j A_\mu^a} = \frac{\pi \alpha_d^2}{18 m_\chi} \eta_d T_d^2 [\ln(\alpha_d^{-1}) + d_0], \quad (20)$$

where $\alpha_d = g^2/(4\pi)$ is the dark fine structure constant, $\eta_d = 2((N-1)^2 - 1)$ is the number of degrees of freedom of the massless gauge bosons in the dark radiation bath, and $d_0 \simeq -1.34 - \ln(N-1)$ for $SU(N-1)$ [37]⁸.

⁸ Here the rate is computed with respect to physical instead of conformal time. The latter is obtained by multiplying the result with a . Furthermore we use a different sign convention for the drag rate as compared to [37].

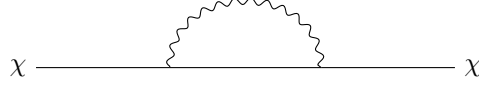


FIG. 5. Self-energy corrections to the dark matter fermion propagator induce the mass splitting between neutral and charged dark matter states after a subset of the gauge bosons in the loop acquire mass via spontaneous symmetry breaking.

A characteristic feature of non-Abelian dark sectors is that, due to the t -channel enhancement, the ratio $\Gamma_{\chi_j A_\mu^a}/H$ is constant during radiation domination, and only slowly decreases afterwards, such that the drag force and the resulting tight coupling between IDM and SIDR can be active over a wide range of redshifts. Phenomenologically this can lead to a suppression of the matter power spectrum over a wide range of scales, allowing for tests with various large-scale structure data sets [29, 30, 37, 55, 57–59]. However, within the model considered here, the IDM-SIDR interaction is effectively switched off at a certain point. This feature of the model is intimately related to the phase transition and the underlying gauge symmetry (breaking), and we turn to this point now.

D. One-loop dark matter mass splitting

The dark matter is affected by the symmetry breaking due to its gauge interaction. Prior to the phase transition, all N components of the dark matter multiplet are degenerate in mass due to the unbroken $SU(N)$ symmetry. After the transition, one-loop corrections to the self-energy of χ lead to a mass splitting (see Fig. 5). Defining as usual the physical mass as the pole of the full propagator, the one-loop correction to the physical mass m can be obtained from the tree-level mass m_0 by solving (with slight abuse of notation, see Appendix C for the precise meaning)

$$[\not{p} - m_0 - \Sigma(\not{p})] |_{\not{p}=m} = 0, \quad (21)$$

and computing the self-energy Σ to one-loop order. The $N-1$ components $\chi_j \equiv (\chi_1, \dots, \chi_{N-1})$ that transform under the remaining unbroken $SU(N-1)$ remain degenerate in mass, but the component $\chi_0 \equiv \chi_N$ that is neutral under $SU(N-1)$ is slightly lighter, with mass splitting

$$\Delta m = c_\Delta \frac{g^3 v}{32\pi}. \quad (22)$$

We illustrate that split in blue in Fig. 2. Here c_Δ is a numerical factor of order unity (see Appendix C). For the case $N=3$ it is $c_\Delta = 1 + 1/\sqrt{3}$. As we see below, this loop-induced mass splitting leads to major phenomenological consequences.

E. Dark radiation matter decoupling

The radiative mass splitting Δm implies that, effectively, dark matter stops to interact with the dark radiation for dark sector temperatures $T_d \ll \Delta m$, as we discuss below. We find this feature to be important for obtaining good agreement with CMB and LSS data for values of H_0 consistent with local measurements, and emphasize that this central prediction is a natural consequence of dark matter being gauged under $SU(N)$. As mentioned before, we refer to this process as dark radiation matter decoupling (DRMD).

Let us first discuss the main features of DRMD, before turning to a more complete discussion of the underlying assumptions. As long as the temperature T_d of the dark sector is (far) above Δm , all N states of the χ multiplet are equally populated. However, once $T_d \ll \Delta m$, the thermal abundance of the heavier charged components χ_j becomes Boltzmann suppressed relative to the lighter one. Since the lighter component χ_0 is neutral under the remaining $SU(N-1)$, it does (practically) not interact with the dark radiation.

The overall χ abundance, parameterized by its constant fraction f_χ of the total dark matter density, is distributed over charged and neutral states,

$$f_\chi = f_{\chi_j}(z) + f_{\chi_0}(z), \quad (23)$$

in a redshift-dependent way. Here $f_{\chi_j}(z)$ stands for the sum over all $N-1$ charged components of χ , and $f_{\chi_0}(z)$ for the neutral one. Directly after the phase transition $T_d \gg \Delta m$, and the charged and neutral states are occupied according

to equipartition, $f_{\chi_0}(z)/f_\chi \simeq 1/N$ and $f_{\chi_j}(z)/f_\chi \simeq (N-1)/N$. Once $T_d \ll \Delta m$, the neutral state is preferred, and we expect $f_{\chi_j}(z)/f_\chi \ll 1$. Indeed, in (Saha) equilibrium the ratio is (using $\Delta m, T_d \ll m_\chi$)

$$\left(\frac{f_{\chi_j}(z)}{f_\chi}\right)_{\text{eq}} = \frac{(N-1)e^{-\Delta m/T_d}}{(N-1)e^{-\Delta m/T_d} + 1} \rightarrow (N-1)e^{-\Delta m/T_d}, \quad (24)$$

where the latter limit applies for $T_d \ll \Delta m$, while equipartition is recovered in the opposite case. A suppression of the χ_j abundance implies that the effective drag rate Γ_{drag} for dark radiation is reduced relative to $\Gamma_{\chi_j A_\mu^a}$ from (20) as

$$\Gamma_{\text{drag}} = \frac{f_{\chi_j}(z)}{f_\chi} \Gamma_{\chi_j A_\mu^a}. \quad (25)$$

While the ratio $\Gamma_{\chi_j A_\mu^a}/H$ is approximately constant, Γ_{drag}/H rapidly decreases once the neutral state is preferred, and if the ratio drops below unity the dark radiation cannot maintain tight coupling to the non-relativistic χ components, giving rise to DRMD.

Let us first estimate the redshift range relevant for DRMD, postponing a more detailed discussion for the moment. As starting point we take the redshift z_{stop} for which the dark sector temperature drops below the mass splitting, i.e. $T_d(z_{\text{stop}}) = \Delta m$. Furthermore, we consider a redshift z_{dec} defined by the requirement that dark matter and dark radiation perturbations cease to be tightly coupled to each other. Provided this occurs due to the reduction of the drag rate, the redshift is set by the time when Γ_{drag}/H drops below unity, as we assume below for definiteness. See once more Fig. 3 for an illustration.

To provide a quantitative estimate, we assume that the fraction of charged states is given by the equilibrium value (24), and parametrize the expansion history conveniently as

$$a^2 H = (a^2 H)|_{\text{after}} \sqrt{1 + \frac{\Omega_m}{\Omega_{\text{rad}}} \frac{1}{1+z}}, \quad (26)$$

where the subscript ‘after’ stands for evaluation after the phase transition at z_* when the dark sector reheating has been completed (during radiation domination). It is given by

$$(a^2 H)|_{\text{after}} = \frac{\pi}{3\sqrt{10}} \frac{1}{M_{\text{pl}}} \sqrt{g_{\text{rel,vis}} + g_{\text{rel,d}} \xi_{*,\text{after}}^4} a^2 T_{\text{vis}}^2. \quad (27)$$

For the redshift z_{stop} at which the exponential suppression kicks in, we read off from (24),

$$\frac{1+z_{\text{stop}}}{1+z_*} = (1+r_g)^{-1/3} \frac{\Delta m}{T_d^{*,\text{after}}}, \quad (28)$$

where the factor $(1+r_g)^{-1/3}$ takes into account the mass threshold effect that occurs at z_t . Noticing from (2) that $m_\psi/\Delta m \sim (32\pi)/g$, the different redshifts satisfy the hierarchy $z_{\text{stop}} \ll z_t \ll z_*$. We can make this more explicit by taking the ratio between (17) and (28),

$$\frac{1+z_t}{1+z_{\text{stop}}} = (1+r_g)^{1/3} \frac{m_\psi}{\Delta m} \simeq \frac{c_\square}{g}, \quad (29)$$

where c_\square is another N -dependent factor that for $N=3$ evaluates to $c_\square = 4 \times 6^{1/6} 7^{1/3} \sqrt{13} (3+\sqrt{3}) \simeq 7.86$ (assuming $\gamma \ll 1$ and using (6) and (22)). In other words, we obtain from (17) and (29) the redshift hierarchy

$$z_* \simeq \frac{c_o}{g} z_t \simeq \frac{c_\square c_o}{g^2} z_{\text{stop}}, \quad (30)$$

which is controlled by the gauge coupling g . The condition $\Gamma_{\text{drag}} = H$ is satisfied even later for $z_{\text{dec}} < z_{\text{stop}}$. Neglecting the second term under the square root in (27), taking $g_{\text{rel,vis}} = 3.38$, and using (14) together with (18), we obtain from (25) (a more explicit derivation is performed in Sec. III A)

$$\frac{1+z_{\text{stop}}}{1+z_{\text{dec}}} \simeq 28 + \ln \left[\frac{16\pi^2 \alpha_d^2}{(0.1)^4} (\ln(\alpha_d^{-1}) + d_0) \left(1 + \frac{\Omega_m}{\Omega_{\text{rad}}} \frac{1}{1+z_{\text{dec}}} \right)^{-1/2} \sqrt{\Delta N_{\text{IR}}} \left(\frac{\text{GeV}}{m_\chi} \right) \right], \quad (31)$$

where we substituted $N = 3$ for illustration. Anticipating our numerical results, we are interested in cases where the decoupling happens close to matter-radiation equality, i.e. $z_{\text{dec}} \sim z_{\text{eq}}$. Therefore, we can estimate $\Omega_m/\Omega_{\text{rad}} \sim z_{\text{dec}}$, and thus ignore the z_{dec} inside the log term. Moreover, we find that $\Gamma_{\text{drag}} \gg H$ is initially satisfied for realistic values of the dark matter mass. To be explicit, we obtain a very weak upper bound on the dark matter mass:

$$m_\chi \lesssim (g/0.1)^4 10^{12} \text{ GeV}. \quad (32)$$

Later, we will see that the DRMD model is efficient at addressing the Hubble tension if $z_{\text{dec}} \sim 1000$. Using (31) and (30) together with $g \lesssim 0.1$, this implies the lower bound $z_* \gtrsim 10^6$. In other words, the decoupling mechanism constrains the phase transition to occur in the redshift window

$$10^6 \lesssim z_* \lesssim 10^9, \quad (33)$$

which slightly tightens the range from [20].

Let us now discuss some refinements and underlying assumptions. The baseline picture followed here assumes kinetic and chemical equilibrium in the dark sector during DRMD at the background level, as well as a tight coupling between the perturbations of charged and neutral states. Kinetic equilibrium within the dark sector at a common temperature T_d for χ_j , χ_0 and A_μ^a relies on exchange of kinetic energy via elastic scatterings, that are efficiently mediated by gauge interactions. An example is the $2 \rightarrow 2$ process $\bar{\chi}_j \chi_0 \rightarrow \bar{\chi}_0 \chi_j$, which can proceed through the s and t -channel exchange of $A^{\pm j}$ and A^0 , respectively [see Fig. 4(c)]. At the same time, apart from momentum, the heavier dark matter states χ_j also exchange energy with the massless gauge bosons in the radiation bath via the scattering $\chi_j A^a \rightarrow \chi_j A^a$, mediated by a A^a [see Fig. 4(a)]. On the other hand, chemical equilibrium in the conversion among charged and neutral states can be established via the inelastic process $\bar{\chi}_j \chi_j \rightarrow \bar{\chi}_0 \chi_0$. It can proceed via the A^0 gauge boson in the s -channel and via t -channel diagrams with exchange of $A^{\pm j}$ [see Fig. 4(b)]. The latter are enhanced due to the t -channel propagator being of order of the momentum transfer (see Appendix D), while the s -channel propagator is suppressed by the dark matter mass. Finally, at the level of perturbations, tight coupling between χ_j and χ_0 relies on momentum exchange, with relevant processes being the same elastic scattering $\bar{\chi}_j \chi_0 \rightarrow \bar{\chi}_0 \chi_j$ as for kinetic equilibration at the background level. Since the relevant rates involving in particular processes with two non-relativistic particles such as $\bar{\chi}_j \chi_0 \rightarrow \bar{\chi}_0 \chi_j$ and $\bar{\chi}_j \chi_j \rightarrow \bar{\chi}_0 \chi_0$ are potentially subject to large (Sommerfeld-)corrections, we defer a detailed analysis of the various processes to future work. For example, it would be interesting to investigate whether DRMD could occur due to the breakdown of tight coupling between χ_0 and χ_j instead of dark radiation and χ_j , as assumed above. Further points are residual interactions of χ_0 with $SU(N-1)$ gauge bosons that could be induced by loop effects (such as electric or magnetic dipole interactions), as well as a breakdown of Saha equilibrium among the χ_0 and χ_j states, similarly as occurs for the later stages of recombination in the visible sector. Finally, it would be worthwhile to consider model extensions, e.g. by adding massless fermion species q charged under $SU(N)$ to the model, that yield a (small) extra contribution to the SIDR component, and mediate further conversion processes between χ_j and χ_0 states, allowing also for $1 \rightarrow 3$ decays such as $\chi_j \rightarrow \chi_0 q^j \bar{q}^0$ that are effective in depleting the charged states down to arbitrarily low temperatures.

Altogether, while a more detailed investigation is of interest, we expect the basic picture of DRMD to be robust: for $T_d \ll \Delta m$ the charged states χ_j become depleted, such that dark radiation stops to interact efficiently with the (then dominantly neutral) χ component at some point. Thus, tight coupling between SIDR and dark matter terminates, increasing the sound velocity for dark radiation while non-Abelian self-interactions keep it from starting to free-stream. As we see below these are important features at the perturbation level for making the model consistent with CMB and BAO data while allowing for a reduction of the sound horizon and thus a large value of H_0 , being generically provided by the model discussed here. Specifically, the redshift z_{stop} at which DRMD dynamics starts is independent of the uncertainties discussed above, while the redshift z_{dec} and the estimate provided in (31) could differ slightly depending on which of the equilibrium conditions discussed above breaks down first.

Overall, guided by fundamental principles we discussed a microscopic model governed by a dark non-Abelian gauge symmetry $SU(N)$, spontaneously broken to $SU(N-1)$ by a Higgs mechanism. We found the latter to predict two key features, being (i) a phase transition in the dark sector that allows to create an SIDR component with sizeable ΔN_{eff} after BBN, and (ii) a mass splitting Δm of a (heavy) fermion charged under the gauge symmetry, providing a tight coupling of SIDR to an interacting dark matter component that terminates once the dark sector temperature drops below Δm . Both of these features play a key role in the way how the model addresses the Hubble tension. We now discuss a setup allowing us to efficiently track the evolution of perturbation modes relevant for a comparison to CMB data.

III. EVOLUTION OF PERTURBATIONS

In this section we work out the evolution of perturbations within the dark sector for the microscopic Hot NEDE model discussed above, and connect its fundamental parameters to those entering the perturbation equations (Sec. III A). For that purpose we extend the setup from [20] by the interacting dark matter component χ . Furthermore, we present a simplified description in Sec. III B, that we refer to as *Dark Radiation Matter Decoupling Model* (DRMD). It captures the essential DRMD dynamics, being applicable if (i) the dark sector phase transition occurs sufficiently early such that perturbation modes observed in the CMB were still outside of the horizon at that time (but still after BBN), requiring roughly $10^6 \lesssim z_* \lesssim 10^9$ (in accordance with (33)), and (ii) the mass-threshold effect at z_t due to the Higgs boson becoming non-relativistic is negligible, which is the case in the large- N limit of $SU(N)$.

A. Dark matter and dark radiation perturbations

We describe perturbations in the dark sector by adding two additional components to the Λ CDM model, one accounting for dark radiation (DR) and one for interacting dark matter (χ). Dark radiation includes the massless gauge bosons, as well as the Higgs as long as it is relativistic. As discussed in [20], non-Abelian self-interactions of gauge bosons as well as interactions of the Higgs allow for a fluid description in terms of the density contrast δ_{DR} and velocity divergence θ_{DR} , suppressing anisotropic stress and higher multipoles. The interacting dark matter component includes the neutral χ_0 and charged χ_j states, assumed to be tightly coupled to each other (see Sec. II E) and being described by a cold (i.e. pressureless) fluid, in line with our assumption $m_\chi \gg T_d$, with density contrast δ_χ and velocity divergence θ_χ . As discussed above we assume that χ contributes as a constant fraction f_χ of the total dark matter density, while the remaining part is taken to be standard CDM (a natural possibility is a further particle species being a singlet under $SU(N)$).⁹ We further use (23) for the redshift-dependent relative abundances in the χ_0 and χ_j states, and moreover assume standard adiabatic initial conditions for all species on superhorizon scales.

The perturbations of the interacting dark matter component in synchronous gauge satisfy (following the notation in [30, 84])

$$\delta'_\chi + \left(\theta_\chi + \frac{h'}{2} \right) = 0, \quad (34a)$$

$$\theta'_\chi + \mathcal{H}\theta_\chi = \mathcal{G}\Delta', \quad (34b)$$

where

$$\Delta' = \theta_{\text{DR}} - \theta_\chi, \quad (35)$$

defines the velocity slip, h is the spatial trace of the metric fluctuation, and \mathcal{G} is a time-dependent function quantifying the momentum transfer between dark matter and dark radiation, related to the drag rate (25), see below for details. Furthermore, primes denote derivative with respect to conformal time τ and $\mathcal{H} = aH$.

Perturbations in the dark radiation fluid are governed by

$$\delta'_{\text{DR}} + (1 + w_{\text{DR}}) \left(\theta_{\text{DR}} + \frac{h'}{2} \right) + 3\mathcal{H}(c_s^2 - w_{\text{DR}}) \delta_{\text{DR}} = 0, \quad (36a)$$

$$\theta'_{\text{DR}} - \frac{k^2 c_s^2}{1 + w_{\text{DR}}} \delta_{\text{DR}} + \mathcal{H}(1 - 3c_s^2) \theta_{\text{DR}} = -\mathcal{G}R\Delta', \quad (36b)$$

where we defined

$$R = \frac{1}{1 + w_{\text{DR}}} \frac{\rho_\chi}{\rho_{\text{DR}}}, \quad (37)$$

and

$$c_s^2 = w_{\text{DR}} - \frac{w'_{\text{DR}}}{3\mathcal{H}(1 + w_{\text{DR}})}, \quad (38)$$

⁹ Since we are interested in a scenario with strong coupling between χ and DR, the case $f_\chi = 1$ is very constrained by data since it generates strong dark acoustic oscillations [29, 30, 40].

is the fluid sound velocity. The factor R arises because we impose conservation of the combined fluid with velocity divergence $(1 + w_{\text{eff}})\rho\theta \equiv (1 + w_{\text{DR}})\rho_{\text{DR}}\theta_{\text{DR}} + \rho_{\chi}\theta_{\chi}$, where $\rho = \rho_{\text{DR}} + \rho_{\chi}$ and w_{eff} is the effective equation of state. Note that we allow for an equation of state $w_{\text{DR}} \neq 1/3$, which arises because the radiation fluid after the phase transition is composed of a mixture of massless gauge bosons and the Higgs that becomes non-relativistic at some point. As mentioned above, the vanishing of higher multipole moments of dark radiation perturbations is a consequence of self-interactions within this sector. Microscopically, those are realized through the gauge interactions of $SU(N)$ [and the residual $SU(N-1)$] before (and after) the phase transition, such as $\psi \leftrightarrow AA$ and $AA \leftrightarrow AA$ [20].

We now describe the cosmological evolution of the dark sector fluids during all epochs resulting from the microscopic model (see Fig. 3) in several steps: the pre-phase transition stage for $z > z_*$, the phase transition at $z = z_*$, and the subsequent evolution, which contains the mass-threshold effect of the Higgs at $z = z_t$ and the later decoupling of χ and DR components at $z_{\text{stop}} \gtrsim z \gtrsim z_{\text{dec}}$.

1. Before the phase transition ($z > z_*$)

Before the phase transition, all $SU(N)$ gauge bosons are massless and as a consequence all χ dark matter degrees of freedom are interacting. Moreover, the (subdominant) dark radiation fluid, composed of $2(N^2 - 1)$ massless gauge bosons and $2N$ highly relativistic Higgs bosons, can be characterized by $c_s^2 = w_{\text{DR}} \simeq 1/3$. We further assume that dark radiation and dark matter are tightly coupled. This is described by the limit $\mathcal{G} \rightarrow \infty$, which simplifies the fluid equations significantly [30, 43]. It follows from (34b) that $\Delta' \rightarrow 0$. We then obtain from (34a) and (36a),

$$\delta_{\chi} = \frac{3}{4}\delta_{\text{DR}} + C^{(-)}, \quad (39)$$

where the integration constant $C^{(-)}$ is vanishing for adiabatic initial conditions. We note that this can be written equivalently as $\Delta = 0$ at leading order in $1/\mathcal{G}$. Taking the difference between (34b) and (36b), it is straightforward to derive the momentum transfer

$$\mathcal{G}\Delta' = 3c_{s,\text{eff}}^2 \left[\frac{k^2}{4}\delta_{\text{DR}} + \mathcal{H}\theta \right], \quad (40)$$

where the sound velocity of the combined fluid is

$$c_{s,\text{eff}}^2 = \frac{1}{3(1+R)}, \quad (41)$$

due to ‘dark matter loading’.

In practical terms, we use (36) together with (40) to evolve the system. The dark matter perturbation δ_{χ} is then obtained from (39). As is well-known from the baryon-photon system, in the tight-coupling limit the interaction enters only indirectly via enforcing the common sound velocity $c_{s,\text{eff}}^2$ and we do not need to specify the interaction rate \mathcal{G} .

2. Phase transition ($z = z_*$)

The first-order phase transition at $\tau = \tau_*$ takes place quasi-instantaneously on cosmological time-scales, and leads to a discontinuous increase in the DR energy density due to the latent heat ΔV being converted into radiation. We therefore have for the background DR density

$$\rho_{\text{DR}}^{(+)} = \rho_{\text{DR}}^{(-)} + \Delta V, \quad (42)$$

where in the supercooled regime $\Delta V \gg \rho_{\text{DR}}^{(-)}$. Here the superscript (\mp) indicates evaluation before and after the phase transition, i.e. $f^{(\mp)} = \lim_{\epsilon \rightarrow 0} f(\tau_* \mp \epsilon)$ for any function $f(\tau)$. This assumes an almost instantaneous energy conversion, which, as discussed in [20], is justified if the Higgs decays into massless gauge bosons efficiently [see also (13)].

This instantaneous conversion is described at the level of perturbations through the matching equations ¹⁰

¹⁰ An intuitive understanding of the matching conditions can be gained through the following argument. Under a general linear diffeomorphism $\xi^{\mu}(\tau, \mathbf{k})$, the two fluid variables transform as $\delta_{\text{DR}} \rightarrow \hat{\delta}_{\text{DR}} = \delta_{\text{DR}} + 4\mathcal{H}\xi^0$ and $\theta_{\text{DR}} \rightarrow \hat{\theta}_{\text{DR}} = \theta_{\text{DR}} - k^2\xi^0$. Consequently, the gauge transformation $(\xi^0)^{(-)} = -\delta_{\text{DR}}^{(-)}/(4\mathcal{H}(\tau_*))$ takes us to a frame where $\hat{\delta}_{\text{DR}}^{(-)} = 0$. Since the phase transition is triggered along a surface of constant $\rho_{\text{DR}}(\tau, \mathbf{x})$, it now occurs simultaneously across space (at least on scales much larger than the typical bubble separation where the stochastic nature of the phase transition can be ignored). As a result, in this ‘trigger frame’, the macroscopic fluid is homogeneously produced and thus both $\hat{\delta}_{\text{DR}}^{(+)} = 0$ and $\hat{\theta}_{\text{DR}}^{(+)} = 0$. Transforming back to the original frame, then recovers (43). This argument assumes that $\rho_{\text{DR}}^{(+)} \gg \rho_{\text{DR}}^{(-)}$, meaning that only the spatial dependence in the trigger surface, i.e. $\delta_{\text{DR}}^{(-)}$, is responsible for the post-phase transition perturbations.

$$\delta_{\text{DR}}^{(+)} = \delta_{\text{DR}}^{(-)}, \quad \theta_{\text{DR}}^{(+)} = -\frac{k^2}{4\mathcal{H}_*} \delta_{\text{DR}}^{(-)}, \quad (43)$$

where we made the simplifying assumption that $w_{\text{DR}}^{(+)} = w_{\text{DR}}^{(-)} = 1/3$. Perturbations $\delta_{\text{DR}}^{(-)}$ in the subdominant dark radiation fluid before the phase transition thus seed perturbations in the dark sector fluid, $\delta_{\text{DR}}^{(+)}$ and $\theta_{\text{DR}}^{(+)}$, after the phase transition, imprinting characteristic features in the matter power spectrum for co-moving scales with wave number $k > \mathcal{H}_*$ [20]. After the phase transition, we assume that tight coupling between the reheated dark radiation fluid and dark matter is quickly restored, i.e. $\theta_\chi \rightarrow \theta_{\text{DR}}^{(+)}$, as a consequence of the efficient momentum transfer between both fluids (see Fig. 4(a) for a microscopic process). In summary, (43) provide the initial conditions for the dark radiation perturbations after the (almost instantaneous) reheating of the dark sector has been completed. The evolution equations (36) along with (40) describing the tightly coupled limit remain valid also after the phase transition. We note that the matching conditions are not required for the simplified model described in Sec. III B.

3. Mass-threshold effect of the Higgs ($z = z_t$)

Another prediction of the Hot NEDE model, described in [20], is a (minor) further increase in ΔN_{eff} (‘second step’), in which the Higgs field becomes non-relativistic. This step vanishes in the large- N limit of $SU(N)$, and was shown to have little influence on the fit to CMB data (see Fig. 8 of [20]) even for $N = 3$. For this reason, we do not implement this second step in the simplified DRMD model (see Sec. III B). We include a description of this second step here for completeness, since it is part of the cosmological history of Hot NEDE, and could hold testable predictions for future higher precision datasets.

The post-phase transition DR fluid consists of $2[(N-1)^2 - 1]$ massless gauge bosons and one massive Higgs degree of freedom in thermal equilibrium. Following [20, 33], this mixed system can be described as a single fluid with time-dependent equation of state parameter

$$w_{\text{DR}}(x) = \frac{1}{3} - \frac{r_g}{3} \frac{\hat{\rho}(x) - \hat{p}(x)}{1 + r_g \hat{\rho}(x)}, \quad (44)$$

where $r_g^{-1} = 2N(N-2)$, and $\hat{\rho}(x)$ and $\hat{p}(x)$ are expressed in terms of modified Bessel functions of the second kind,

$$\begin{aligned} \hat{\rho}(x) &= \frac{K_1(x)}{6} x^3 + \frac{K_2(x)}{2} x^2, \\ \hat{p}(x) &= \frac{K_2(x)}{2} x^2. \end{aligned} \quad (45)$$

The relation between a and $x = m_\psi/T_d$ can then be obtained by numerically solving

$$\left(\frac{xa_t}{a}\right)^3 = 1 + \frac{r_g}{4} (3\hat{\rho}(x) + \hat{p}(x)), \quad (46)$$

which imposes entropy conservation of the combined fluid. Here $a_t \equiv 1/(1+z_t)$ corresponds to the scale factor where the Higgs becomes non-relativistic. As shown in (17), the redshift ratio z_t/z_* is parametrically controlled by g . In particular, for $z_t \ll z_*$, the Higgs is highly relativistic with $x \ll 1$ and the above equations yield $w_{\text{DR}} \simeq 1/3$ in agreement with the assumptions made for the perturbation matching in (43).

Physically, these equations describe how the (dark) Higgs boson, when it becomes non-relativistic and annihilates, heats the dark radiation fluid, leading to an increase in ΔN_{eff} . According to (18), the size of this second step is quantified in terms of r_g and vanishes for $N \rightarrow \infty$.

4. Dark matter decoupling ($z_{\text{stop}} > z > z_{\text{dec}}$)

As a new feature of this work, we include the interaction of the dark radion fluid with dark matter. As discussed in Sec. II, due to the mass splitting Δm between the neutral and the $(N-1)$ charged components of the χ multiplet, the interaction rate receives an additional time-dependent Boltzmann suppression. As a result, the charged sector is depopulated as $T_d < \Delta m$, which in turn suppresses the interaction rate and hence \mathcal{G} . Since $\Delta m \sim g^3 v \ll m_\psi \ll T_d^*$, this happens after the phase transition and the second step at $z = z_t$. To describe this stage, we cannot use the tight

coupling approximations and go back to the separate set of evolution equations for DR (36) and χ (34). This requires to explicitly specify the interaction rate \mathcal{G} , which we discuss in the following.

For easier comparison with the literature, we specify the relation with the ETHOS framework [39]. To be specific, the parameter \mathcal{G} is related to the opacity $\Gamma_{\text{DR-idm}}$ through $\mathcal{G} \equiv -\frac{1}{R}\Gamma_{\text{DR-idm}}$, which is conventionally parametrized as

$$\Gamma_{\text{DR-idm}} = -(\Omega_\chi h^2) x_{\text{idm}}(z) \sum_{n \geq 0} a_n \left(\frac{1+z}{1+z_D} \right)^n. \quad (47)$$

Our case is captured by the choice $a_{n>0} = 0$. The coefficient a_0 is related to the microscopic parameters in the previous section through

$$\begin{aligned} a_0 &= \frac{a R}{\Omega_{\text{idm}} h^2} \Gamma_{\chi_j A_\mu^a} \\ &= \frac{a R}{\Omega_{\text{idm}} h^2} \frac{\pi \alpha_d^2}{18 m_\chi} \eta_d T_d^2 (\ln(\alpha_d^{-1}) + d_0), \end{aligned} \quad (48)$$

which, except for a mass threshold effect around $z = z_t$, is indeed constant during radiation domination because $T_d \propto 1/a$ and $R \propto a$ (as $w_{\text{DR}}(\tau) \simeq 1/3$). The factor $x_{\text{idm}}(z)$ accounts for any additional time-dependence. In particular, it captures the Boltzmann suppression of the charged dark matter component χ_j ,

$$x_{\text{idm}}(z) = \frac{f_{\chi_j}(z)}{f_\chi} x_{\text{back}}(z) = \frac{(N-1)e^{-\Delta m/T_d}}{(N-1)e^{-\Delta m/T_d} + 1} x_{\text{back}}(z), \quad (49)$$

where we assumed the equilibrium ratio (24) and used that the number density of a single non-relativistic degree of freedom is $n_1 \simeq 2\sqrt{2}\pi^{3/2}e^{-T_d/m}(T_d/m)^{3/2}$. The factor x_{back} absorbs deviations of the expansion history from pure radiation domination. We then obtain

$$\mathcal{G} = (\Omega_\chi h^2) \frac{a_0}{R} x_{\text{idm}}(z). \quad (50)$$

Right after the phase transition, we have $\Delta m \ll T_d$ and $x_{\text{back}} \simeq 1$, and thus

$$\left(\frac{\mathcal{G}}{\mathcal{H}} \right) \Big|_{\text{after}} \simeq \frac{N-1}{N} (\Omega_\chi h^2) \left(\frac{a_0}{\mathcal{H}R} \right) \Big|_{\text{after}}. \quad (51)$$

As we are interested in a situation where $(\mathcal{G}/\mathcal{H})_* \gg 1$, we can employ the tight-coupling approximation, which makes the fluid evolution initially insensitive to the precise redshift-dependence of \mathcal{G} . Eventually, at some later redshift $z \ll z_t$, we have $\Delta m \gg T_d$, and (49) yields

$$\left(\frac{\mathcal{G}}{\mathcal{H}} \right) \simeq N \left(\frac{\mathcal{G}}{\mathcal{H}} \right) \Big|_{\text{after}} x_{\text{back}}(z) e^{-\Delta m/T_d}, \quad (52)$$

where we read off

$$x_{\text{back}}(z) = \frac{a_0}{a_0|_{\text{after}}} \frac{(\mathcal{H}R)|_{\text{after}}}{\mathcal{H}R} = (1+r_g)^{2/3} \left(1 + \frac{\Omega_m}{\Omega_{\text{rad}}} \frac{1}{1+z} \right)^{-1/2}, \quad (53)$$

which accounts for both the mass threshold effect at $z = z_t$ and deviations from radiation domination. For our later Boltzmann evolution, it is therefore useful to introduce

$$\left[\frac{\mathcal{G}}{\mathcal{H}} \right]_{\text{ini}} = N (1+r_g)^{2/3} (\mathcal{G}/\mathcal{H}) \Big|_{\text{after}} \quad (54)$$

as the input parameter.¹¹ It can be related to the microscopic parameters introduced in Sec. II through [37]

$$\begin{aligned} \left[\frac{\mathcal{G}}{\mathcal{H}} \right]_{\text{ini}} &= (N-1) \frac{a_*^2 \Gamma_{\chi_j A_\mu^a}}{a_* \mathcal{H}_*} \\ &= \frac{\sqrt{10}}{3} \frac{(N-1)((N-1)^2-1)}{\sqrt{g_{\text{rel,vis}} + g_{\text{rel,d}} \xi_{*,\text{after}}^4}} \alpha_d^2 (\ln(\alpha_d^{-1}) + d_0) \xi_{*,\text{after}}^2 (1+r_g)^{2/3} \frac{M_{\text{pl}}}{m_\chi}, \end{aligned} \quad (55)$$

¹¹ We note that this assumes that the tight-coupling approximation is still valid when $\Delta m \sim T_d$. Otherwise, one needs to use the full expression in (49) to describe the decoupling.

where in the second line, we substituted (20) and used (27) written in conformal time. Neglecting the second term under the square root, taking $g_{\text{rel,vis}} = 3.38$, and using (14) together with (18), we obtain

$$\left[\frac{\mathcal{G}}{\mathcal{H}}\right]_{\text{ini}} \simeq 1.5 \times 10^{12} \frac{(N-1)\sqrt{(N-1)^2-1}}{2\sqrt{3}} \frac{16\pi^2\alpha_d^2}{(0.1)^4} (\ln(\alpha_d^{-1}) + d_0) \sqrt{\Delta N_{\text{IR}}} \left[\frac{\text{GeV}}{m_\chi}\right]. \quad (56)$$

We further parametrize the full time-dependence (valid for $\Delta m \gg T_d$) as

$$\mathcal{G} \simeq \mathcal{H} \left(\frac{\mathcal{G}}{\mathcal{H}}\right)_{\text{ini}} \left(1 + \frac{\Omega_m}{\Omega_{\text{rad}}} \frac{1}{1+z}\right)^{-1/2} \exp\left(-\frac{1+z_{\text{stop}}}{1+z}\right), \quad (57)$$

where we used the redshift z_{stop} at which the exponential suppression kicks in defined in (28). Requiring that $\mathcal{G}/\mathcal{H} = 1$ at $z = z_{\text{dec}}$ yields

$$\frac{1+z_{\text{stop}}}{1+z_{\text{dec}}} \simeq \ln\left(\left[\frac{\mathcal{G}}{\mathcal{H}}\right]_{\text{ini}}\right). \quad (58)$$

Substituting (56) for $N = 3$, we recover the numerical estimate given in (31).

A priori, the microscopic model parameters are the gauge coupling g , the choice of gauge group N , the VEV v , the effective Higgs mass μ_{eff} , and the dark matter mass m_χ supplemented with the initial dark sector temperature ξ and the fraction of χ dark matter f_χ . These microscopic parameters can be traded for the phenomenological parameters ΔN_{IR} , z_{stop} , z_* , r_g and $(\mathcal{G}/\mathcal{H})_{\text{ini}}$, introduced above. To have a first test of the decoupling feature against cosmological data, we introduce a simplified model in the next section and leave a full exploration of the Hot NEDE phenomenology for future work.

B. Dark radiation matter decoupling model

As mentioned before, the simplified DRMD model arises from the Hot NEDE model in the large- N limit of $SU(N)$ and for a phase transition redshift $10^6 \lesssim z_* \lesssim 10^9$, in agreement with the bounds in (33). We recall that here we impose the upper bound to ensure that the phase transition occurs after BBN, and thereby satisfy BBN constraints on ΔN_{eff} . Modes that are observed in CMB or LSS data are, during these early times, still frozen outside the horizon, and it is sufficient to impose adiabatic initial conditions for the post-phase transition fluid, effectively eliminating z_* as a free parameter. Moreover, $r_g \rightarrow 1$ for $N \rightarrow \infty$, which means that the ‘second step’ in ΔN_{eff} from the mass-threshold effect of the Higgs is negligible. We are therefore left with the additional parameters $\Delta N_{\text{IR}} = \Delta N_{\text{NEDE}} \equiv \Delta N_{\text{eff}}$, f_{idm} , z_{stop} and $(\mathcal{G}/\mathcal{H})_{\text{ini}}$. The DRMD model is thus a four-parameter extension of Λ CDM. Later, we will see that $(\mathcal{G}/\mathcal{H})_{\text{ini}}$ is unconstrained by current datasets, making the model effectively a three-parameter extension of Λ CDM. Here we employ the conventional notation $f_{\text{idm}} = f_\chi = f_{\chi_0} + f_{\chi_j}$ for denoting the (conserved) fraction of χ dark matter, and $\delta_{\text{idm}} \equiv \delta_\chi$ as well as $\theta_{\text{idm}} \equiv \theta_\chi$ for density and velocity perturbations, respectively. As far as CMB/LSS perturbation modes are concerned, the only non-trivial feature that makes this simplified model different from (post-BBN) SIDR is the time-dependent interaction between dark radiation and dark matter. In particular, in the limit where $f_{\text{idm}} \rightarrow 0$, both parameters z_{stop} and $(\mathcal{G}/\mathcal{H})_{\text{ini}}$ become unconstrained and the DRMD model reduces to SIDR.¹² In summary, the DRMD and the SIDR model are phenomenological descriptions of the Hot NEDE model for large z_* and N , corresponding to the case with and without interacting dark matter, respectively.

We implement standard adiabatic initial conditions for superhorizon modes with wavenumber $k\tau \ll 1$. In synchronous gauge, they read [84]

$$\frac{4}{3}\delta_{\text{idm}} = \delta_{\text{DR}} = \delta_\gamma = \delta_\nu = -\frac{2}{3}Ck^2\tau^2, \quad (59)$$

where C is an integration constant that can be matched to the (conserved) co-moving curvature perturbation and δ_γ and δ_ν are the photon and neutrino density contrast. Solving the coupled perturbation equations for the metric (h, η) and fluid perturbations $(\delta_g, \delta_{\text{idm}}, \delta_\nu, \delta_{\text{DR}}, \theta_{\text{idm}}, \theta_\nu, \theta_{\text{DR}}, \theta_g)$ at leading nontrivial order in $k\tau$, we obtain the following initial conditions for the dark radiation and dark matter velocity perturbations (in agreement with the results in [53])

$$\theta_{\text{DR}} = \theta_\gamma = -\frac{1}{18}Ck^4\tau^3, \quad (60)$$

¹² Later we will see that the same degeneracy leads to strong projection effects when performing a Bayesian parameter extraction for the DRMD model. We therefore perform also a profile likelihood analysis.

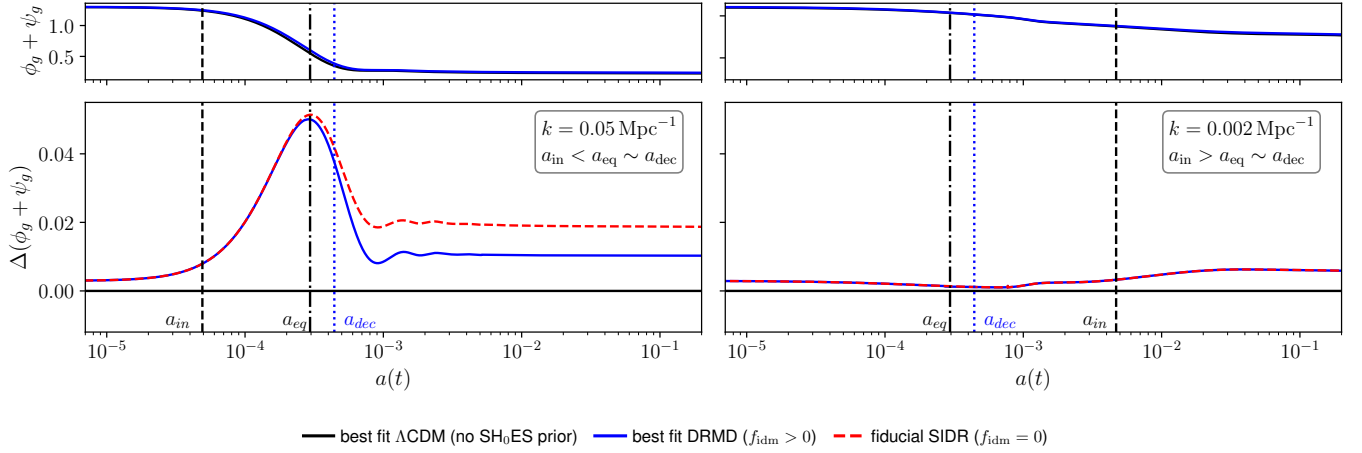


FIG. 6. Evolution of the Weyl potential $\phi_g + \psi_g$ for a mode that entered the horizon (a_{in}) before (left panel) and after (right panel) matter-radiation equality (a_{eq}). In the lower panel we normalize the amplitudes with respect to the Λ CDM best fit cosmology (without SH_0ES prior). The blue line is the DRMD best fit (with SH_0ES prior). For explicit parameter values refer to Tab. II. The red dashed line corresponds to a fiducial SIDR cosmology with the same best fit parameters as the DRMD cosmology except for $f_{\text{idm}} = 0$. In that case, the large value of H_0 is penalized by a net enhancement of the gravitational potential for pre-equality modes (left panel). The decoupling feature of the DRMD model compensates this effect while keeping the post-equality mode invariant, provided decoupling (a_{dec}) occurs around matter-radiation equality. Accordingly, in the right panel, SIDR and DRMD agree.

and

$$\theta_{\text{idm}} = \frac{(\mathcal{G}/\mathcal{H})_{\text{ini}}}{4 + (\mathcal{G}/\mathcal{H})_{\text{ini}}} \theta_\gamma. \quad (61)$$

In particular, we find $\theta_{\text{idm}} \rightarrow 0$ for $\mathcal{G}/\mathcal{H} \rightarrow 0$ as expected for dark matter perturbations in synchronous gauge [84] and $\theta_{\text{idm}} = \theta_{\text{DR}}$ in the tight-coupling limit $\mathcal{G}/\mathcal{H} \rightarrow \infty$. We can also check that for superhorizon modes the adiabatic initial conditions and the perturbation matching in (43) become indistinguishable, up to corrections that are suppressed by powers of $k\tau$.

Let us stress that the DRMD model can also be understood as a rather general phenomenological model, which might admit other microscopic realizations. At face value, it describes the decoupling between (self-interacting) dark radiation and a fraction of dark matter through an initially strong interaction that shuts off exponentially. Importantly, here the dark radiation remains fluid-like also after this decoupling (in contrast to photons after decoupling from baryons, and in contrast to atomic dark matter [47–51]), and ΔN_{eff} is constant from before the onset of the decoupling process until $z = 0$ (in contrast to [53], for which the step in ΔN_{eff} plays a central role in improving the fit to CMB data).

The main effect of the decoupling between dark matter and dark radiation is that modes that entered the horizon after $z = z_{\text{dec}}$, i.e. modes with wavenumber $k \lesssim \mathcal{H}(z_{\text{dec}})$, evolve as they would in a standard SIDR scenario without interactions. Modes with $k \gtrsim \mathcal{H}(z_{\text{dec}})$, on the other hand, ‘feel’ the effects of the interaction. In particular, dark matter perturbations receive a small positive pressure as they are dragged along by dark radiation, which suppresses the gravitational potential and hence the matter power spectrum on those scales. In practical terms, this means that the DRMD model can efficiently compensate for effects that enhance the gravitational potential on small scales. In particular, addressing the Hubble tension through an energy injection in the primordial fluid requires increasing¹³ $\omega_m = \Omega_m h^2$ by up to 15%. Such an increase is problematic. For example, it leads to an earlier onset of matter domination, which in turn reduces the net decay of the gravitational potential for any mode that entered the horizon *before* matter domination. This effect can be seen by comparing the left and right panels in Fig. 6, which show the evolution of the sum of the gravitational potentials ψ_g and ϕ_g in conformal Newtonian gauge (adopting the convention in [84]) for a pre- and post-phase transition mode, respectively. In both models, SIDR (red dashed) and DRMD (blue), there

¹³ This can be understood by a simple geometrical argument: The inverse angular size of the sound horizon (at photon decoupling) $r_s \approx r_d$ is given by $\theta_s^{-1} \simeq \frac{1}{H_0 r_s} \int_0^{z_{\text{rec}}} dz [\Omega_m(1+z)^3 + (1-\Omega_m)]^{-1}$. Now, the angular scale θ_s and $H_0 r_s$ are constrained model-independently at the sub-permille [8] and the sub-percent level [12], respectively. As we consider models that leave the physics of recombination unchanged, z_{rec} is fixed to its Λ CDM value. This implies that Ω_m can only deviate from its Λ CDM value by a few percent, and thus increasing h by around 8% to resolve the Hubble tension is accompanied by a $> 10\%$ increase in $\omega_m = \Omega_m h^2$.

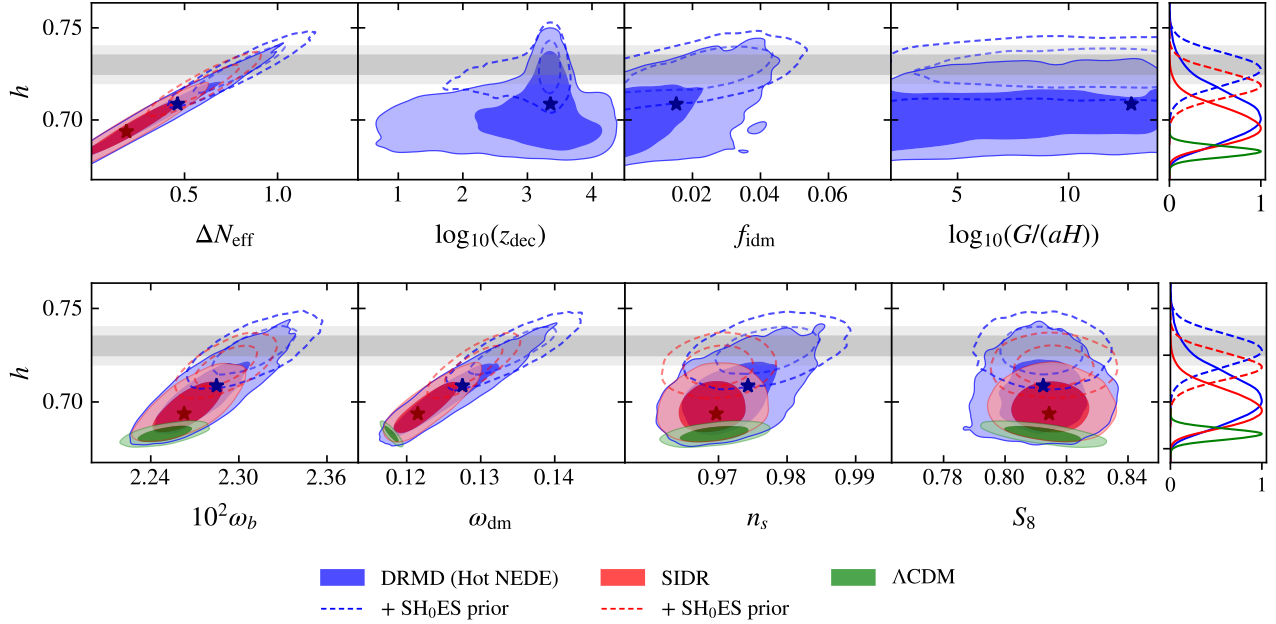


FIG. 7. Marginalized posteriors are shown for our baseline data combination, consisting of Planck 2018, DESI BAO (DR2), and (uncalibrated) Pantheon+ SNe data, as filled contours. The dashed contours additionally include a SH_0ES prior. Dark and light shaded regions correspond to 68% C.L. and 95% C.L., respectively. The first and second row display DRMD and ΛCDM model parameters, respectively. The DRMD model (blue) shows better agreement with the SH_0ES measurement (gray bands) than SIDR (red) if the decoupling between dark matter and dark radiation occurs at $z_{\text{dec}} \sim 2000$. Notably, the DRMD contours exhibit strong projection effects when marginalized over the $\log_{10}(z_{\text{dec}})$ direction, e.g. compare the second with the third panel in the first row. As is common in early-time solutions to the Hubble tension, h is strongly correlated with ω_b , ω_{dm} , and the spectral tilt n_s . Best fit values of the baseline DRMD and SIDR run, taken from Tab. II, are indicated as blue and red stars, respectively.

is an enhancement of the gravitational potential. As a consequence, the success of these models relies crucially on their ability to counter the effects of an increase in ω_m . While this is achieved through different mechanisms such as delaying matter domination or having sizeable dark sector acoustic oscillations (see [16, 85] for more details), the interactions between dark matter and dark radiation in the DRMD model provide an additional mechanism operative on scales $k \gtrsim \mathcal{H}(z_{\text{dec}})$. This is visualized in Fig. 6, which compares the best fit DRMD cosmology with a fiducial SIDR cosmology (red dashed) with the same parameter values, except that dark radiation in the SIDR model does not interact with dark matter, i.e. $f_{\text{idm}} = 0$. It can be seen that in the DRMD model the enhancement of the gravitational potential is (partially) compensated, leading to a smaller amplitude of the gravitational potential for pre-equality modes (left panel) compared to SIDR. This mechanism is particularly effective if the decoupling occurs during the early stage of matter domination, because then the modes most affected by the increase in ω_m are subjected to the effects of the interaction, i.e. an excess decay of the gravitational potential. We will see in the next section that this expectation, i.e. $z_{\text{dec}} \sim z_{\text{eq}}$, is confirmed by our parameter extraction, when testing the model against a canonical set of cosmological data.

IV. RESULTS

In this section, we first describe the data sets and analysis strategy, and then present our results. We focus on the DRMD model to describe the dark sector, and compare it to the SIDR and ΛCDM models.

A. Data analysis

We have implemented the *Dark Radiation Matter Decoupling Model* (DRMD) in the Boltzmann solver CLASS [43], dubbed DRMD-CLASS. It is publicly available on github¹⁴, and includes a component of self-interacting dark radiation (i.e. described by a fluid) and an additional interacting dark matter component, with background densities characterized by the parameters ΔN_{eff} and the fraction f_{idm} , respectively. Importantly, the dark radiation component is assumed to be generated after BBN. In practical terms, this means that we take the Λ CDM value for N_{eff} when computing the primordial Helium fraction from BBN. The interaction between dark radiation and dark matter is parametrized through (57). It is characterized by two additional model parameters, being the redshift z_{stop} at which exponential suppression of the DR-IDM drag rate \mathcal{G} relative to the Hubble rate \mathcal{H} sets in, and the initial ratio $(\mathcal{G}/\mathcal{H})_{\text{ini}}$ at $z \gtrsim z_{\text{stop}}$. The decoupling redshift z_{dec} is then already fixed by (58). For evolving the perturbations, we use the equations in (36a) and (34a) with $w_{\text{DR}} = c_s^2 = 1/3$, in accordance with the assumption that the dark Higgs gives a negligible contribution to dark radiation within the simplified DRMD model. As initial conditions, we use (59), (60) and (61). We use the DRMD-CLASS implementation to simulate the Λ CDM ($\Delta N_{\text{eff}} = f_{\text{idm}} = 0$), the SIDR ($f_{\text{idm}} = 0$), and the DRMD cosmology. The extra parameters compared to Λ CDM are ΔN_{eff} for SIDR and $\Delta N_{\text{eff}}, f_{\text{idm}}, z_{\text{stop}}, (\mathcal{G}/\mathcal{H})_{\text{ini}}$ for DRMD.

For our data analysis, we use the following datasets (later referred to as ‘base’):

- **Planck 2018**: CMB anisotropy measurements, which include lensing, high- ℓ TT+TE+EE and low- ℓ TT+EE data [8, 86].
- **DESI BAO**: Release 2 (DR2) BAO data obtained from three years of measurement by the DESI collaboration [12].¹⁵
- **Pantheon+**: SNe data, based on a catalog of 1550 Type Ia SNe over the redshift range $0.001 < z < 2.26$ [44].

We also carry out complementary runs, where we include the local determination of H_0 by the SH₀ES collaboration [1] (referred to as ‘base + SH₀ES prior’). We implement this constraint as a Gaussian prior on the SNe Type Ia absolute magnitude, which is $M = -19.253 \pm 0.027$ (corresponding to $H_0 = 73.04 \pm 1.04$ km/s/Mpc).

We perform a Monte Carlo Markov Chain (MCMC) analysis with the `MontePython` package [87, 88], employing its implementation of the Metropolis-Hastings algorithm. We include as free parameters the six Λ CDM parameters consisting of the (dimensionless) baryon density $\omega_b = \Omega_b h^2$, the total dark matter density $\omega_{\text{dm}} = \Omega_{\text{dm}} h^2$, comprised of cold and interacting dark matter, the Hubble parameter $h = H_0/(100 \text{ km/sec/Mpc})$, the primordial scalar power spectrum amplitude $\log_{10}(A_s)$ and tilt n_s , and the optical depth to reionization τ_{reio} . All of them are varied within wide prior ranges. Following the Planck 2018 convention, the neutrino sector is described in terms of two massless and one massive neutrino with mass $m_3 = 0.06 \text{ eV}$ and temperature $T_3 = 0.716 \text{ eV}$, amounting to $N_{\text{eff}}^{\Lambda\text{CDM}} = 3.046$. In the case of the SIDR model, we also sample the additional relativistic density in the form of a (non-free-streaming) fluid component, parameterized in terms of $\Delta N_{\text{eff}} \in [0, 3]$, i.e., the total effective neutrino number is $N_{\text{eff}} = N_{\text{eff}}^{\Lambda\text{CDM}} + \Delta N_{\text{eff}}$. In the case of the DRMD model, these parameters are supplemented with the fraction of interacting dark matter $f_{\text{idm}} \in [0, 1]$, the redshift at which the exponential suppression occurs $\log_{10}(z_{\text{stop}}) \in [2, 5]$, and the initial value of the opacity $\log_{10}(\mathcal{G}/\mathcal{H})_{\text{ini}} \in [2, 14]$, where for simplicity we drop the subscript ‘ini’ when presenting results. The prior is chosen such that we always ensure to be in a tight-coupling regime when the suppression at $z = z_{\text{stop}}$ starts. Moreover z_{dec} is inferred from the code as a ‘derived parameter’ using the definition $(\mathcal{G}/\mathcal{H})|_{z=z_{\text{dec}}} = 1$.

The resulting chains are analyzed with `GetDist` [89] and considered converged when the Gelman-Rubin criterion drops below at least $R - 1 = 0.05$ [90]. For assessing the residual Hubble tension of a given model, we employ the *difference in maximum a posteriori* (DMAP) statistics [91]. It is defined as $Q_{\text{DMAP}}^M = \sqrt{\chi^2(\text{Base}) - \chi^2(\text{Base} + M \text{ prior})}$ and has the benefit of being insensitive to prior volume effects while reproducing the usual result for Gaussian posteriors. It has become the standard for analyzing Early Universe solutions to the Hubble tension and in particular EDE-type models that are known to exhibit non-Gaussian posteriors [22, 45]. We also use the Akaike Information Criterion (AIC) $\Delta\text{AIC} = \Delta\chi^2 + 2\Delta\text{d.o.f.}$ as a way to penalize extra degrees of freedom compared to Λ CDM.

Our Bayesian analysis is complemented by a common frequentist approach. It relies on computing the likelihood \mathcal{L} of the data for a given choice of model parameters. To be specific, we employ the `Procolli` package [92] to obtain *profile likelihood* curves, which sample the maximal \mathcal{L} along a given axis in parameter space.

¹⁴ <https://github.com/NEDE-Cosmo/DRMD-CLASS.git>.

¹⁵ We use an updated version of the DESI implementation in <https://github.com/LauraHerold/MontePython.desilike>.

	Base				Base + SH ₀ ES prior				Q_{DMAP}^M	Q_{Gauss}
	H_0	ΔN_{eff}	$\Delta\chi^2$	ΔAIC	H_0	ΔN_{eff}	$\Delta\chi^2$	ΔAIC		
ΛCDM	68.30 ± 0.29	–	–	–	68.70 ± 0.29	–	–	–	5.7σ	4.4σ
SIDR	$69.8^{+0.8}_{-1.0}$ (69.4)	< 0.525 (0.188)	-1.2	0.8	71.9 ± 0.7 (72.0)	0.61 ± 0.13 (0.610)	-24.5	-22.5	3.0σ	2.5σ
DRMD	$70.5^{+1.0}_{-1.6}$ (70.9)	< 0.811 (0.462)	-3.0	3.0	72.8 ± 0.8 (72.9)	0.80 ± 0.16 (0.829)	-33.3	-27.3	1.4σ	1.8σ

TABLE I. Comparison between ΛCDM , (post-BBN) SIDR, and DRMD (Hot NEDE) as solutions to the Hubble tension, using standard metrics. While SIDR reduces the QDMAP tension to 3σ , the DRMD model brings it to below 2σ . The (naive) Gaussian tension measure is reported in the last column. After including a prior on M , we report a 4.7σ and 5σ evidence for a non-vanishing fraction of ΔN_{eff} for SIDR and DRMD, respectively. For a complete account of our cosmological parameter inference see Tab. II.

B. Results discussion

As a major result of this work we find that the DRMD model is able to fully resolve the Hubble tension. In particular, we report a small value of DMAP given by 1.4σ , and hence consistent with statistical fluctuations.¹⁶ For ΛCDM , the DMAP tension is 5.7σ , in agreement with the standard Hubble tension result. For the SIDR model, that we consider for comparing to our results, the DMAP metric yields a significant alleviation, but leaving a residual 3σ tension, in broad accordance with previous analyses of non-free-streaming extra radiation that is created after BBN [20, 22, 32, 33, 52, 83, 93, 94]. Thus, the feature of dark radiation matter decoupling within the DRMD model has a decisive impact on the evolution of perturbations, allowing for a significant reduction of the sound horizon, and thus increase in the inferred H_0 , while remaining consistent with CMB, BAO and SNe data. The main results of our MCMC analysis are presented in Tab. I. A more comprehensive table, including mean values, uncertainties, best-fit points, and corresponding χ^2 values, is provided in Appendix A. When considering the Gaussian tension, calculated assuming Gaussian posterior in H_0 , the tension is reduced from 4.4σ to 2.5σ in SIDR and to 1.8σ in DRMD.

The DRMD base analysis provides us with the upper bound $\Delta N_{\text{eff}} < 0.811$ (95% C.L.), corresponding to an increased mean value for the Hubble parameter of $H_0 = 70.5^{+1.0}_{-1.6}$ km/s/Mpc (68% C.L.), alongside a fit improvement compared to ΛCDM of $\Delta\chi^2 = -3$ (given the number of free parameters this is at an expected level for the base analysis, i.e. without including local H_0 data; otherwise this becomes $\Delta\chi^2 = -33.3$, see below). This is a clear improvement over SIDR, which leads to the tighter constraint $\Delta N_{\text{eff}} < 0.525$ (95% C.L.) and hence a smaller increase in H_0 . This can also be seen in Fig. 7 where the filled blue contours corresponding to the DRMD base analysis fully overlap with the SH₀ES constraints (within their 95% C.L.), although the latter has not been used in the base analysis. This figure also shows the positive correlations with the ΛCDM parameters ω_b , ω_{dm} , and n_s that are typical for Early Universe solutions to the Hubble tension. However, in contrast to other EDE-type models such as axiEDE [27] (but notable not Cold NEDE [19]), the value of S_8 does not increase. Instead, it is almost unchanged compared to ΛCDM . We attribute this to the presence of a small fraction $f_{\text{idm}} < 3.6\%$ (95% C.L.) of interacting dark matter, which suppresses power on small scales that enter the horizon before $z = z_{\text{dec}}$.

It is important to stress that the DRMD analysis suffers from relatively strong projection effects. This can best be seen in the second panel of the first row in Fig. 7, where the best fit value, which we indicate as a blue star, lies vertically aligned with the narrow ridge around $\log_{10}(z_{\text{dec}}) = 3.4$ that extends to remarkably high values of H_0 . This feature would be missed in the other panels that marginalize over $\log_{10}(z_{\text{dec}})$ (see also the 1D posterior in the last panel to the right). We therefore decided to complement our Bayesian analysis with profile likelihood plots, which we present in Fig. 1. Here the left panel corresponds to our baseline (with no prior on M). Compared to ΛCDM , we see that the SIDR model’s main effect is to enlarge the width of the 1D profile likelihood, corresponding to an approximate degeneracy between ΔN_{eff} and H_0 . However, this degeneracy is far from perfect and reaching values of $H_0 \sim 73$ km/s/Mpc is still penalized with a $\Delta\chi^2 \sim 10$ (in agreement with a 3σ residual tension). Moreover, the global best fit value remains close to its ΛCDM counterpart. This situation changes drastically for the DRMD model. The profile curve becomes very flat, introducing an almost perfect degeneracy between H_0 and $(f_{\text{idm}}, \Delta N_{\text{eff}})$. At the same time, the global best fit moves to higher values around $H_0 = 71$ km/s/Mpc. We also indicate the corresponding 1σ and 2σ lines, which in agreement with the DMAP tension indicate an insignificant sub- 2σ residual tension. We stress that this result does not use any local constraints on the expansion rate and is instead driven by CMB, BAO, and (uncalibrated) SNe data alone.

¹⁶ We emphasize that our analysis always combines BAO, SNe, and CMB data, and is therefore insensitive to possible ‘internal’ tensions among these individual datasets. In particular, the reported 1.4σ DMAP value refers specifically to the level of agreement between this combined baseline and SH₀ES alone. At this stage, we do not investigate how the recently found [12] 2.3σ discrepancy in Ω_m between DESI DR2 and Planck data is affected within the DRMD and SIDR model.

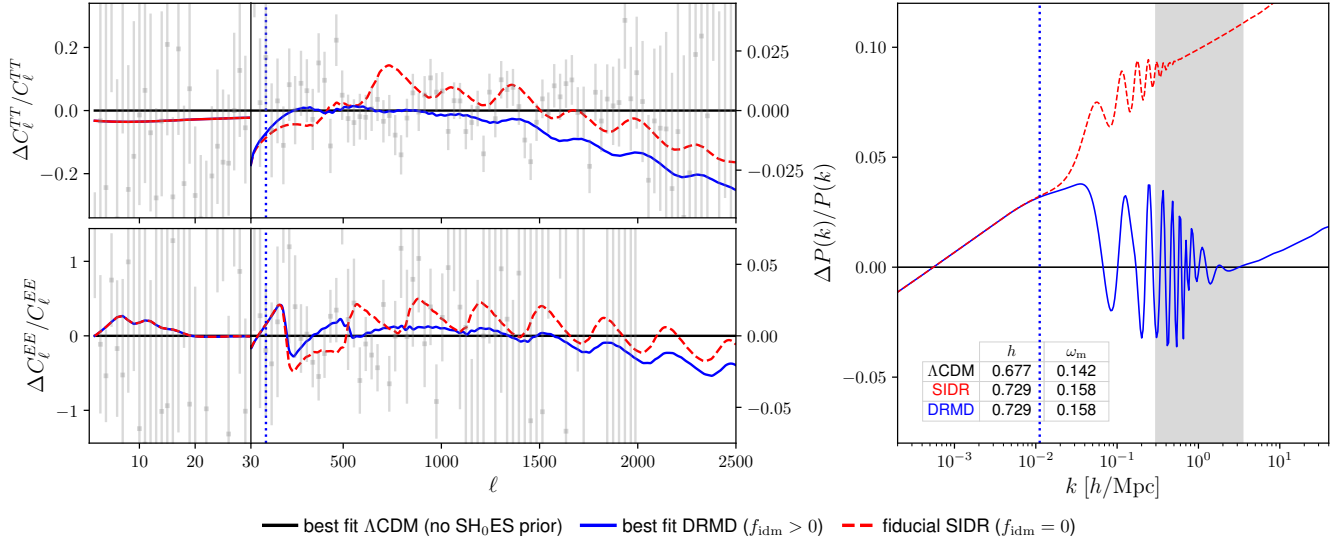


FIG. 8. CMB temperature and polarization residuals (left), and the matter power spectrum (right), are shown for the DRMD best-fit cosmology (base with a SH_0ES prior), relative to the ΛCDM base cosmology (base without a SH_0ES prior). The red dashed line represents a fiducial SIDR model using the same DRMD best-fit parameters but with $f_{\text{idm}} = 0$. In the DRMD model, modes to the left of the vertical dotted line have entered the horizon after dark radiation decoupled from dark matter at $z = z_{\text{dec}}$. This decoupling feature suppresses small-scale power, allowing the model to accommodate large values of $h \simeq 0.73$ without enhancing the matter power spectrum. Parameter values are listed in Tab. II. The two y-axes in the left panel refer to the low and high- ℓ range separated by the black vertical line.

In the case of the DRMD model, these previous findings justify a combined analysis that includes the SH_0ES prior on M (referred to as ‘Base + SH_0ES ’). It leads to a relatively high value of the expansion rate of $H_0 = 72.8 \pm 0.8 \text{ km/s/Mpc}$ (68% C.L.), which comes alongside a remarkable 5σ evidence for a non-vanishing ΔN_{eff} and a significant fit improvement of $\Delta\chi^2 = -33.3$. The corresponding posteriors are displayed as the dashed contours in Fig. 7. While becoming generically tighter and moving to slightly higher values of H_0 , overall, the DRMD constraints are not changed drastically by including the SH_0ES prior (much less than in the case of SIDR, which still exhibits a 3σ residual tension). In particular, the redshift of dark matter radiation decoupling is only mildly affected and still corresponds to a value close to matter-radiation equality, in agreement with the general discussion in Sec. III B. Overall, the late decoupling around $z_{\text{dec}} \approx 2200$ (using the best fit in Tab. II) proves to be a rather robust prediction of our model. The relevance of the decoupling mechanism is also reflected by the fact that in the presence of the SH_0ES prior the constraints on the interacting dark matter fraction relaxes to $f_{\text{idm}} < 4.4\%$ (95% C.L.), enabling larger values of H_0 . Correspondingly, Fig. 1 shows a degeneracy between H_0 and f_{idm} .

On the other hand, the initial coupling strength $\log_{10}(\mathcal{G}/\mathcal{H})_{\text{ini}}$ is mostly unconstrained. This can be attributed to the fact that for $\mathcal{G}/\mathcal{H} \gg 1$ the dynamics of perturbations becomes universal as \mathcal{G} can be eliminated from the perturbation equations through (40). The only way, it still affects the data fit is at a later stage when tight coupling is no longer a valid approximation and \mathcal{G}/\mathcal{H} in (57) approaches values of order unity (around $z \sim z_{\text{dec}}$), although it is highly degenerate with z_{stop} . To be specific, by constraining the value of z_{dec} , due to (31), only the ratio $\ln(\mathcal{G}/\mathcal{H})_{\text{ini}}/(1+z_{\text{stop}})$ is determined. This implies we can trade a larger value of $\log_{10}(\mathcal{G}/\mathcal{H})_{\text{ini}}$ for a larger value of z_{stop} . In principle, this degeneracy is not perfect, as for example the derivative $d\mathcal{G}/dz|_{z=z_{\text{dec}}}$ does depend on a different parameter combination. However, as we see in Fig. 7, data is almost insensitive to this aspect. This also justifies not to discriminate between different decoupling scenarios. As a consequence, we can think about the DRMD model as a three-parameter extension of ΛCDM that beyond ΔN_{eff} and f_{idm} only depends on $(1+z_{\text{dec}})^{-1} = \ln(\mathcal{G}/\mathcal{H})_{\text{ini}}/(1+z_{\text{stop}})$.¹⁷ This might however change with future data sets. Let us stress that breaking this degeneracy would allow us to constrain the value of α_d^2/m_χ through (31) and thus directly learn about the range of allowed dark matter masses. Very tentatively, the best fit values in Fig. 1 point towards a slight preference for values around $\log_{10}(\mathcal{G}/\mathcal{H})_{\text{ini}} \approx 12$, which due to (56) corresponds to a sub-GeV dark matter mass.

In order to better understand how the DRMD model affects cosmological observables, we show in Fig. 8 the CMB temperature and polarization residuals (left) alongside the matter power spectrum (right) for the DRMD best fit

¹⁷ This is also the reason why in Fig. 7 we choose to present the results in terms of the derived parameter z_{dec} rather than z_{stop} .

cosmology (blue line), relative to the base Λ CDM model (black line). To highlight the relevant features, we consider the DRMD analysis that includes a SH_0ES prior. Notably, ω_m is 12% larger than in the Λ CDM reference cosmology. As argued before, this increase enables a large value of $h \simeq 73$ without shifting the CMB peaks. Despite this drastic change in the background cosmology, the power spectra remain comparable to Λ CDM. In particular, the matter power spectrum does not show a strong enhancement as one could naively expect when ω_m is increased as much. We attribute this to the effect of the interactions between dark radiation and dark matter that suppress power on small scales. To illustrate this aspect further, we also included a fiducial SIDR cosmology (red dashed) that uses the same parameter values as the DRMD model but sets $f_{\text{idm}} = 0$. In this case, power is generically enhanced on scales that entered the horizon after the decoupling at $z = z_{\text{dec}}$ – represented by the vertical dotted line. Moreover, the fiducial SIDR cosmology exhibits more pronounced oscillatory residuals in the CMB spectra compared to the DRMD model, suggesting that the model struggles to accommodate similarly large values of H_0 . In addition, we note the presence of dark acoustic oscillations in the matter power spectrum of DRMD. This represents an important feature that can be directly probed in the short future by redshift surveys, as done in the context of BOSS and eBOSS [95–98].

Finally, let us stress that so far we have tested the model against a canonical set of cosmological data. From Fig. 8, we see that the temperature power spectrum for the DRMD (and SIDR) model deviates most significantly from Λ CDM on small scales. As a result, we expect that new large- ℓ data as for example provided recently by ACT [11, 99] and SPT [10] can test and constrain our scenario further.¹⁸ The same applies to future constraints on the full shape of the matter power spectrum from DESI. We leave a detailed investigation for future work.

V. CONCLUSIONS

We present and analyze a dark sector model described by a simple Lagrangian that is based on renowned principles of particle physics, featuring a non-Abelian gauge symmetry and spontaneous symmetry breaking via a Higgs mechanism, and find that it provides a full solution to the Hubble tension within standard current data sets. We refer to an implementation capturing the key features as DRMD model, while the full model is based on the Hot NEDE framework.

From a cosmological point of view, the non-Abelian gauge bosons provide a thermal bath of self-interacting dark radiation. The associated extra relativistic energy density yields a potential mechanism to decrease the sound horizon and thereby enable a larger value of H_0 inferred from the position of acoustic peaks in CMB and BAO data, as compared to Λ CDM. However, as is well-known, adding this extra energy without further modifications, known as SIDR model, is by itself not sufficient to resolve the Hubble tension, being disfavoured by (i) its impact on CMB polarization and temperature perturbations as well as (ii) BBN constraints.

As we show in this work, the feature of spontaneous symmetry breaking within the dark sector simultaneously addresses both of these shortcomings. First, as already noticed in [20], the phase transition associated to symmetry breaking reheats the dark sector, reconciling the cosmic evolution with BBN if the transition occurs between BBN and CMB epochs. Second, adding a fermion multiplet charged under the gauge symmetry yields a component of dark matter that interacts with the thermal bath of gauge bosons. Spontaneous symmetry breaking induces a small mass splitting among the neutral and charged components of the multiplet, implying that this interaction terminates once the dark sector temperature drops below the mass splitting, while the self-interactions within the dark radiation bath remain active due to the non-Abelian self-coupling of gauge bosons. We find that this feature of dark radiation matter decoupling (DRMD) impacts the evolution of perturbations such that CMB polarization and temperature anisotropies as well as BAO are consistent with standard current data sets, while allowing for (and even slightly preferring) a significant dark radiation density and thus an increase in the inferred H_0 value. Specifically, we find 1.4σ agreement between the combined Planck 2018, DESI DR2, Pantheon+ data sets and SH_0ES within a simplified three-parameter implementation of the DRMD model, while they are in tension at 5.7σ in Λ CDM and 3.0σ for SIDR.

From a theoretical standpoint, we stress that the Hot NEDE model provides several non-trivial key features for solving the Hubble tension that follow from a straightforward microscopic model, with well-known dynamics operating at energy scales in the eV-100keV regime close to those of the visible sector, and a Lagrangian given by standard ingredients within particle physics. For comparison, while Cold NEDE¹⁹ is perfectly natural from an Effective Field Theory (EFT) point of view, featuring very light Axion-Like Particles (ALPs) and GUT scale vacuum expectation values (as is typical for ALP-like models), the involved energy scales are much larger and smaller, respectively, than the energy scale of the NEDE phase transition solving the Hubble tension, and also very different from the energy scales of the visible sector.

¹⁸ While this was done recently for axiEDE [100, 101], we stress that the DRMD model, due to its unique decoupling feature, can lead to different conclusions.

¹⁹ The axiEDE model [26] features Planckian axion decay constants and vacuum expectation values within an arguably exotic potential, which is more challenging for embeddings into quantum gravity [28], although perhaps not impossible at the cost of some fine-tuning [102].

Our work motivates several directions for further investigation, such as an analysis of the DRMD model against recent high resolution CMB data from ACT [99] and SPT [10]. Furthermore, in light of future CMB and LSS data, it would be interesting to take into account further features predicted by the model, that are not considered in the simplified DRMD implementation. These can allow for a discrimination against other proposed solutions of the Hubble tension such as Cold NEDE and axiEDE, and include the direct imprint of the dark sector phase transition on perturbations at small scales, leading to features in the matter power spectrum, as well as the mass-threshold effect of the Higgs. Moreover, low-frequency gravitational waves produced during the phase transition provide a potential further signal, which is specially interesting in light of the recent PTA results [75, 76]. From the particle physics perspective, a refined analysis of the decoupling dynamics as well as a study of the Early Universe history and the population of the dark sector, for example via (gravitational) freeze-in, are of interest.

Acknowledgements

We acknowledge support by the Excellence Cluster ORIGINS, which is funded by the Deutsche Forschungsgemeinschaft (DFG, German Research Foundation) under Germany's Excellence Strategy – EXC-2094 - 390783311. FN was supported by VR Starting Grant 2022-03160 of the Swedish Research Council. We acknowledge Aleksandr Charchyan, Lorenzo De Ros and Elisa Ferreira for useful conversations. MSS acknowledges Nordita and MIAPbP for their hospitality and stimulating environments during the completion of parts of this work.

Appendix A: Table with MCMC results

	Λ CDM		SIDR		DRMD	
	Base	Base + SH ₀ ES prior	Base	Base + SH ₀ ES prior	Base	Base + SH ₀ ES prior
Parameter	68% limits (best fit)	68% limits (best fit)	68% limits (best fit)	68% limits (best fit)	68% limits (best fit)	68% limits (best fit)
$10^2 \omega_b$	2.250 ± 0.012 (2.243)	2.261 ± 0.013 (2.263)	2.266 ± 0.016 (2.263)	2.291 ± 0.014 (2.292)	$2.277^{+0.017}_{-0.026}$ (2.285)	2.310 ± 0.018 (2.313)
ω_{dm}	0.11795 ± 0.00064 (0.11923)	0.11710 ± 0.00062 (0.11705)	$0.1228^{+0.0024}_{-0.0034}$ (0.1215)	0.1290 ± 0.0026 (0.1291)	$0.1259^{+0.0034}_{-0.0061}$ (0.1275)	0.1344 ± 0.0037 (0.1353)
h	0.6828 ± 0.0029 (0.6771)	0.6874 ± 0.0028 (0.6877)	$0.6978^{+0.0076}_{-0.010}$ (0.6937)	0.7192 ± 0.0071 (0.7195)	$0.705^{+0.010}_{-0.016}$ (0.709)	0.7276 ± 0.0082 (0.7289)
$\ln(10^{10} A_s)$	3.054 ± 0.015 (3.048)	3.059 ± 0.016 (3.063)	3.048 ± 0.015 (3.049)	$3.042^{+0.014}_{-0.016}$ (3.039)	3.051 ± 0.015 (3.051)	$3.050^{+0.015}_{-0.017}$ (3.050)
n_s	0.9694 ± 0.0033 (0.9671)	0.9718 ± 0.0033 (0.9730)	0.9692 ± 0.0034 (0.9697)	0.9700 ± 0.0034 (0.9697)	$0.9721^{+0.0039}_{-0.0055}$ (0.9743)	0.9770 ± 0.0048 (0.9783)
τ_{reio}	$0.0611^{+0.0070}_{-0.0078}$ (0.0567)	0.0639 ± 0.0078 (0.0655)	$0.0604^{+0.0068}_{-0.0077}$ (0.0598)	$0.0607^{+0.0068}_{-0.0081}$ (0.0595)	$0.0611^{+0.0071}_{-0.0080}$ (0.0610)	$0.0618^{+0.0068}_{-0.0084}$ (0.0609)
ΔN_{eff}	–	–	< 0.525 (0.188)	0.61 ± 0.13 (0.61)	< 0.811 (0.462)	0.80 ± 0.16 (0.83)
f_{idm}	–	–	–	–	< 0.0362 (0.0152)	< 0.0442 (0.0285)
$\log_{10}(\mathcal{G}/\mathcal{H})$	–	–	–	–	unconstrained (12.823)	unconstrained (13.057)
$\log_{10}(z_{\text{stop}})$	–	–	–	–	> 2.50 (4.82)	> 3.64 (4.83)
$\log_{10}(z_{\text{dec}})$	–	–	–	–	$3.03^{+0.75}_{-0.34}$ (3.36)	$3.25^{+0.22}_{-0.12}$ (3.35)
S_8	0.8125 ± 0.0084 (0.8242)	0.8043 ± 0.0084 (0.8057)	0.8151 ± 0.0086 (0.8143)	0.8157 ± 0.0085 (0.8146)	0.8120 ± 0.0096 (0.8124)	0.8120 ± 0.0089 (0.8115)
$hr_d[\text{Mpc}]$	100.72 ± 0.48 (99.70)	101.46 ± 0.47 (101.51)	101.03 ± 0.52 (100.93)	101.69 ± 0.47 (101.71)	100.95 ± 0.53 (100.96)	101.24 ± 0.52 (101.13)
Ω_m	0.3026 ± 0.0037 (0.3104)	0.2970 ± 0.0035 (0.2967)	0.3001 ± 0.0040 (0.3009)	0.2950 ± 0.0035 (0.2949)	0.3009 ± 0.0040 (0.3007)	0.2987 ± 0.0039 (0.2995)
χ^2 per experiment						
Planck high- ℓ	2348.8	2351.7	2348.9	2354.4	2347.2	2349.5
Planck low- ℓ EE	397.7	399.3	397.3	397.2	397.7	397.6
Planck low- ℓ TT	22.6	22.3	22.5	22.3	21.8	21.3
Planck lensing	9.2	9.3	9.3	9.6	9.4	9.5
DESI BAO	12.8	10.4	11.8	10.4	11.6	11.0
Pantheon+	1412.7	1414.1	1413.1	1414.5	1413.1	1413.4
SH ₀ ES	–	29.6	–	3.4	–	0.6
Total	4203.9	4236.6	4202.9	4211.8	4200.9	4203.0
$\Delta\chi^2$	0.0	0.0	-1.0	-24.8	-3.0	-33.6
$Q_{\text{DMAP}}^M [\sigma]$	–	5.7	–	3.0	–	1.4

TABLE II. Results of our MCMC analysis for Λ CDM, SIDR and DRMD. The base data sets consists of Planck 2018, DESI BAO (DR2), and Pantheon+. The SH₀ES measurement is implemented through a prior on the SNe magnitude M . We report the 1σ standard deviation (except for one-sided constraints, which correspond to the 2σ limit).

Appendix B: Dark matter interacting via spontaneously broken $SU(N)$

In this appendix we provide some details on the mass spectrum and interaction within the dark sector.

We choose a basis in (dark) $SU(N)$ color space such that the Higgs vacuum expectation value (VEV) is aligned with the N th component of the Higgs field Ψ ,

$$\langle \Psi \rangle = (0, \dots, 0, v)/\sqrt{2}. \quad (\text{B1})$$

1. Gauge bosons

In the unbroken theory, gauge bosons are massless and couple according to the $SU(N)$ generators t^A for $A = 1, \dots, N^2 - 1$,

$$D_\mu = \partial_\mu - ig t^A A_\mu^A. \quad (\text{B2})$$

Inserting the Higgs VEV into the kinetic term of the Higgs in the Lagrangian yields the mass terms for gauge bosons after symmetry breaking,

$$\mathcal{L}_{\text{gauge boson mass}} = \frac{1}{2} g^2 v^2 (t^A t^B)_{NN} A_\mu^A A^{B\mu}. \quad (\text{B3})$$

We obtain a mass matrix for the gauge bosons. To analyze it, we consider the generators t^A . The $N^2 - 1$ generators of the full $SU(N)$ group can be split in three categories:

$$t^A = \underbrace{\begin{pmatrix} & & & 0 \\ & t^a & & \vdots \\ & & 0 & \\ 0 & \dots & 0 & 0 \end{pmatrix}}_{\substack{\text{adj of } SU(N-1) \\ a=1, \dots, (N-1)^2 - 1}}, \quad \underbrace{\frac{1}{2} \begin{pmatrix} 0 & \dots & 0 & \\ \vdots & \ddots & \vdots & \mathbf{e}_j \\ 0 & \dots & 0 & \\ \mathbf{e}_j^T & & & 0 \end{pmatrix}}_{\substack{\text{complex fund. of } SU(N-1) \\ j=1, \dots, N-1}}, \quad \underbrace{\frac{1}{2} \begin{pmatrix} 0 & \dots & 0 & \\ \vdots & \ddots & \vdots & i\mathbf{e}_j \\ 0 & \dots & 0 & \\ -i\mathbf{e}_j^T & & & 0 \end{pmatrix}}_{\substack{\text{complex fund. of } SU(N-1) \\ j=1, \dots, N-1}}, \quad (\text{B4})$$

$$\underbrace{\frac{1}{\sqrt{2N(N-1)}} \begin{pmatrix} 1 & & & 0 \\ & \ddots & & \vdots \\ & & 1 & 0 \\ 0 & \dots & 0 & -(N-1) \end{pmatrix}}_{\text{singlet of } SU(N-1)},$$

where $\mathbf{e}_1^T = (1, 0, \dots, 0), \dots, \mathbf{e}_{N-1}^T = (0, \dots, 0, 1)$ are the $N - 1$ dimensional unit basis vectors. The generators are normalized as usual, $\text{tr}(t^A t^B) = \delta^{AB}/2$.

We accordingly split the gauge fields into three categories,

$$\begin{array}{llll} \text{adj.} & A_\mu^a & a = 1, \dots, (N-1)^2 - 1 & \text{massless,} \\ \text{fund.} & A_\mu^{\pm j} & j = 1, \dots, N-1 & m_{A^\pm} = gv/2, \\ \text{sing.} & A_\mu^0 & & m_{A^0} = gv\sqrt{\frac{N-1}{2N}}. \end{array} \quad (\text{B5})$$

The masses follow from inserting the generators into the mass term. Here we define $A_\mu^{\pm j} \equiv \frac{1}{\sqrt{2}}(A_\mu^{\mathbf{e}_j} \pm iA_\mu^{i\mathbf{e}_j})$ where the gauge fields are those associated to the generators involving \mathbf{e}_j and $i\mathbf{e}_j$, respectively. Indeed, the mass term reads

$$\mathcal{L}_{\text{gauge boson mass}} = m_{A^\pm}^2 A_\mu^{+j} A_\mu^{-j} + \frac{1}{2} m_{A^0}^2 A_\mu^0 A^{0\mu}. \quad (\text{B6})$$

Later we also need some knowledge about triple gauge boson self-interactions. The only non-zero interactions are of the form adj.-³, adj.-fund.-fund., sing.-fund.-fund., see Appendix E.

2. Interacting dark matter

We consider interacting dark matter described by a Dirac fermion multiplet χ , that transforms in the fundamental representation of $SU(N)$,

$$\mathcal{L} \supset \bar{\chi}(i\not{D} - m_\chi)\chi, \quad (\text{B7})$$

with mass $m_\chi \gg gv$, making up a fraction f_{idm} of the total cold dark matter abundance. After spontaneous symmetry breaking, we have to discriminate the components in the N -direction, and the remaining $N - 1$ components that transform under the unbroken $SU(N - 1)$ subgroup,

$$\chi = (\underbrace{\chi_1, \dots, \chi_{N-1}}_{\text{fund. } \chi_j}, \underbrace{\chi_N}_{\text{sing.}, \chi_0}). \quad (\text{B8})$$

Loop corrections lead to a mass splitting, making the singlet slightly lighter for the relevant cases with $N > 2$ (see Appendix C)

$$\Delta m_\chi = m_{\chi_j} - m_{\chi_0} = \frac{g^3 v}{32\pi} (N - 2) \left(1 + \sqrt{\frac{2}{N(N - 1)}} \right). \quad (\text{B9})$$

The interactions follow from writing out the covariant derivative in the kinetic term, and inserting the decomposition of gauge bosons. We get

$$\mathcal{L} \supset g \bar{\chi} t^A \not{A} \chi = g \bar{\chi}_i t_{ij}^a A_\mu^a \chi_j + \frac{g}{\sqrt{2}} \left(\bar{\chi}_0 \not{A}^{-j} \chi_j + \bar{\chi}_j \not{A}^{+j} \chi_0 \right) + g \left(q_f \bar{\chi}_j \not{A}^0 \chi_j + q_0 \bar{\chi}_0 \not{A}^0 \chi_0 \right), \quad (\text{B10})$$

with $q_f = 1/\sqrt{2N(N - 1)}$ and $q_0 = -(N - 1)q_f$. From this one can read off the gauge interactions. Note that only the heavier states χ_j interact with the massless gauge bosons A_μ^a .

Appendix C: Computation of mass splitting

Loop corrections lead to a mass splitting between the first $N - 1$ and the last state. This effect is analogous to the Higgsino and Wino mass splitting, and we can compute it in an analogous way, see e.g. [42]. Here we consider the leading one-loop contribution, and the limit $m_A \ll m_\chi$. The one-loop self-energy diagram with an exchange of a gauge boson reads, in Feynman gauge²⁰

$$i\Sigma_{ab} = (ig)^2 (t^A t^A)_{ab} \int \frac{d^d l}{(2\pi)^d} \gamma^\mu \frac{i}{\not{p} + \not{l} - m_\chi} \gamma^\nu \frac{-ig_{\mu\nu}}{l^2 - m_A^2}. \quad (\text{C3})$$

Here we sum over $A = 1, \dots, N^2 - 1$ gauge bosons, each with mass m_A . The indices $a, b = 1, \dots, N$ correspond to the color indices of the in- and outgoing χ lines, respectively. In the unbroken phase, all $m_A = 0$, and the sum over A gives the unit matrix $(t^A t^A)_{ab} = C_F \delta_{ab}$ with a constant C_F . This means the self-energy is diagonal in color space in the unbroken phase. Thus the one-loop correction to the χ mass is identical for all components $a = 1, \dots, N$ before the symmetry breaking. After symmetry breaking, the masses m_A are different for the various gauge bosons $A = 1, \dots, N^2 - 1$. This leads to a mass splitting. Since we are only interested in the splitting relative to each other, it is sufficient to compute (we omit indices ab for brevity)

$$\Delta\Sigma = \Sigma - \Sigma|_{m_A=0}. \quad (\text{C4})$$

²⁰ In R_ξ gauge, $-ig_{\mu\nu} \mapsto -ig_{\mu\nu} + i(1 - \xi)l_\mu l_\nu / (l^2 - \xi m_A^2)$. The additional contribution gives a loop integral

$$\int d^d l \frac{l(\not{p} + \not{l} + m_\chi)l(1 - \xi)}{((p + l)^2 - m_\chi^2)(l^2 - m_A^2)(l^2 - \xi m_A^2)}. \quad (\text{C1})$$

Using $\{\gamma_\mu, \gamma_\nu\} = 2g_{\mu\nu}$, the enumerator can be rewritten as

$$l(\not{p} + \not{l} + m_\chi)l = ((p + l)^2 - p^2)l - (\not{p} - m_\chi)l^2. \quad (\text{C2})$$

For computing the (on-shell) mass splitting we set $p^2 = m_\chi^2$, such that the contribution involving $(p + l)^2 - p^2 = (p + l)^2 - m_\chi^2$ cancels the χ propagator in the denominator, and the resulting loop integral vanishes since the integrand is odd under $l \rightarrow -l$. The contribution proportional to $\not{p} - m_\chi$ also does not give a contribution to the on-shell mass correction. The naive argument is that it vanishes due to the Dirac equation when acting on an on-shell spinor, $\not{p}u_p = m_\chi u_p$. The more precise argument is that any correction to the self-energy proportional to $\not{p} - m_\chi$ yields equal correction to the mass and kinetic terms, see (C5) below, and thus their contributions to the mass shift cancel each other. Thus, the ξ -dependent part of the loop does not contribute to the (on-shell) mass, and the results in R_ξ and Feynman gauge agree. This is consistent with gauge invariance of on-shell masses.

We can generally decompose the self-energy into a correction of the kinetic and of the mass term as

$$\Delta\Sigma = \not{p}\Sigma^K(p^2) - m_\chi\Sigma^M(p^2). \quad (C5)$$

The one-loop mass shift is (see e.g. [42])

$$\Delta m_{ab} = (\Sigma^M(m_\chi^2) - \Sigma^K(m_\chi^2))m_\chi. \quad (C6)$$

To compute it, we anticipate that the result cannot be divergent, and set $d = 4$ except in terms that are divergent in intermediate steps of the computation. We first rewrite the self-energy as

$$i\Sigma_{ab} = -ig^2(t^A t^A)_{ab} [(-2\not{p} + 4m_\chi)I_0 - 2\gamma_\mu I_1^\mu], \quad (C7)$$

where

$$I_0 \equiv -i \int \frac{d^d l}{(2\pi)^d} \frac{1}{(p+l)^2 - m_\chi^2} \frac{1}{l^2 - m_A^2}, \quad (C8)$$

$$I_1^\mu \equiv -i \int \frac{d^d l}{(2\pi)^d} \frac{l^\mu}{(p+l)^2 - m_\chi^2} \frac{1}{l^2 - m_A^2}. \quad (C9)$$

Lorentz invariance implies $I_1^\mu = p^\mu I_1(p^2)$ with a scalar integral $I_1(p^2) = \frac{p^\mu}{p^2} I_1^\mu$. Thus, at one-loop, comparing to (C5) gives

$$\begin{aligned} \Sigma^M(p^2) &= 4g^2(t^A t^A)_{ab} \Delta I_0 \\ \Sigma^K(p^2) &= 2g^2(t^A t^A)_{ab} (\Delta I_0 + \Delta I_1) \end{aligned}$$

where $\Delta I_0 = I_0 - I_0|_{m_A=0}$ and similar for I_1 . A standard computation gives

$$I_0 = \frac{\Gamma(2-d/2)}{16\pi^2} \int_0^1 dx [xm_\chi^2 + (1-x)m_A^2 - x(1-x)p^2]^{d/2-2}. \quad (C10)$$

For $d \rightarrow 4$ the Gamma function has a pole, but also the exponent of the square bracket goes to zero. Expanding the square bracket around $d = 4$ shows that the divergence is independent of the masses and momenta. Thus it cancels in ΔI_0 . Using $(d/2-2)\Gamma(2-d/2) \rightarrow 1$ for $d \rightarrow 4$ gives

$$\Delta I_0 = -\frac{1}{16\pi^2} \int_0^1 dx \{ \ln [xm_\chi^2 + (1-x)m_A^2 - x(1-x)p^2] - \ln [xm_\chi^2 - x(1-x)p^2] \}. \quad (C11)$$

Setting $p^2 = m_\chi^2$ to obtain the mass splitting, and expanding for $m_A \ll m_\chi$, yields

$$\Delta I_0 = -\frac{1}{16\pi^2} \frac{\pi m_A}{m_\chi} + \mathcal{O}\left(\frac{m_A^2}{m_\chi^2}\right). \quad (C12)$$

One can show similarly that ΔI_1 starts only at order m_A^2 . Thus at leading order in m_A/m_χ ,

$$\begin{aligned} \Sigma^M(p^2 = m_\chi^2) &= -4 \frac{g^2}{16\pi} (t^A t^A)_{ab} \frac{m_A}{m_\chi} \\ \Sigma^K(p^2 = m_\chi^2) &= -2 \frac{g^2}{16\pi} (t^A t^A)_{ab} \frac{m_A}{m_\chi} \end{aligned}$$

and therefore

$$\Delta m_{ab} = -\frac{g^2}{8\pi} (t^A t^A)_{ab} m_A. \quad (C13)$$

This contains a sum over all $A = 1, \dots, N^2 - 1$ dark gauge bosons, and is a mass-matrix in (dark) color space.

Taking the example of $N = 3$, and using the Gell-Mann matrices $t^A = \lambda^A/2$, as well as the masses $m_{A_1} = m_{A_2} = m_{A_3} = 0, m_{A_4} = m_{A_5} = m_{A_6} = m_{A_7} = gv/2, m_{A_8} = gv/\sqrt{3}$, one finds

$$(t^A t^A)_{ab} m_A = \frac{gv}{4} \begin{pmatrix} 1 & & \\ & 1 & \\ & & 2 \end{pmatrix} + \frac{gv}{12\sqrt{3}} \begin{pmatrix} 1 & & \\ & 1 & \\ & & 4 \end{pmatrix}. \quad (C14)$$

Thus the mass matrix is diagonal, and gives an equal mass shift to the $a = 1$ and $a = 2$ components as required by the remaining $SU(2)$ symmetry after the phase transition. However, the component $a = 3$ receives a more negative mass correction, and is therefore lighter. This is the neutral state under $SU(2)$. Thus, the splitting between the $a = 1, 2$ and $a = 3$ is

$$\Delta m = \Delta m_{11} - \Delta m_{33} = \Delta m_{22} - \Delta m_{33} = \frac{g^3 v}{32\pi} \left(1 + \frac{1}{\sqrt{3}} \right). \quad (\text{C15})$$

For general N , we use (B4) and see that the sum of generators corresponding to the fundamental under $SU(N-1)$ gives $\sum t^A t^A|_{\text{fund}} = 1/2 \text{diag}(1, \dots, 1, N-1)$, and $t^A t^A|_{\text{sing.}} = 1/(2N(N-1)) \text{diag}(1, \dots, 1, (N-1)^2)$. This means the mass matrix Δm_{ab} is diagonal, and splits into a correction to the mass of the first $N-1$ components χ_j for $a = b = 1, \dots, N-1$ (the fundamental under $SU(N-1)$) and the last component $a = b = N$, $\chi_N \equiv \chi_0$. Altogether,

$$\begin{aligned} \Delta m_{\chi_j} &= -\frac{g^2}{8\pi} \left(\frac{1}{2} m_{A^\pm} + \frac{1}{2N(N-1)} m_{A^0} \right), \\ \Delta m_{\chi_0} &= -\frac{g^2}{8\pi} \left(\frac{N-1}{2} m_{A^\pm} + \frac{(N-1)^2}{2N(N-1)} m_{A^0} \right). \end{aligned} \quad (\text{C16})$$

This yields for the relative mass splitting

$$\Delta m = \Delta m_{\chi_j} - \Delta m_{\chi_0} = \frac{g^3 v}{32\pi} (N-2) \left(1 + \sqrt{\frac{2}{N(N-1)}} \right). \quad (\text{C17})$$

Appendix D: Computation of conversion cross section

Consider $\chi_j \bar{\chi}_j \rightarrow \chi_0 \bar{\chi}_0$ via t -channel exchange of $A_\mu^{\pm j}$. The matrix element for $\chi_i(p_1) \bar{\chi}_j(p_2) \rightarrow \chi_0(q_1) \bar{\chi}_0(q_2)$ averaged over colors i, j and initial spins, and summed over final spins reads

$$|\overline{\mathcal{M}^2}| = \frac{g^4}{(N-1)(t - m_{A^\pm}^2)^2} \left(4m_\chi^2(m_\chi + \Delta m)^2 - 2m_\chi(m_\chi + \Delta m)(p_1 q_1 + p_2 q_2) + 2p_1 p_2 q_1 q_2 + 2p_1 q_2 p_2 q_1 \right), \quad (\text{D1})$$

where $t = (p_1 - q_1)^2$. We assume that all in- and outgoing states are non-relativistic and $\Delta m \propto g^3 v \ll m_\chi$. Then we can approximate all summands in the numerator with m_χ^4 , up to corrections that are relative suppressed by $\Delta m/m_\chi$ or by powers of the velocities,

$$|\overline{\mathcal{M}^2}| = \frac{4g^4 m_\chi^4}{(N-1)(t - m_{A^\pm}^2)^2}. \quad (\text{D2})$$

For evaluating the cross section, and the t variable, we introduce a parameterization of the 4-momenta in the center of mass frame. In the center of mass frame $p_{1,2} = ((m_\chi + \Delta m_\chi)(1 + (v_{\text{rel}}/2)^2/2), \pm(m_\chi + \Delta m_\chi)\mathbf{v}_{\text{rel}}/2)$ and $q_{1,2} = (m_\chi(1 + (v'_{\text{rel}}/2)^2/2), \pm m_\chi \mathbf{v}'_{\text{rel}}/2)$. Energy conservation fixes the relative velocity in the final state to be

$$v'_{\text{rel}}{}^2 = v_{\text{rel}}^2 + \frac{8\Delta m}{m_\chi}. \quad (\text{D3})$$

Here we neglected terms of order $v_{\text{rel}}^2 \times \Delta m/m_\chi$, being consistent with the assumed power counting. We are in fact interested in the conversion at temperatures of the dark sector T_d in the ballpark of Δm . Assuming the interacting dark matter is in kinetic equilibrium, this means $m_\chi v_{\text{rel}}^2 \sim T_d$, thus both terms on the right-hand side of (D3) need to be kept. The differential cross section is

$$\frac{d\sigma}{dt} = \frac{1}{64\pi s} \frac{1}{\mathbf{p}_1^2} |\overline{\mathcal{M}^2}|. \quad (\text{D4})$$

The boundaries for t are $t_{0,1} = -(|\mathbf{p}_1| \mp |\mathbf{q}_1|)^2$. Using $(t_0 - t_1)/\mathbf{p}_1^2 = 4|\mathbf{q}_1|/|\mathbf{p}_1| = 4v'_{\text{rel}}/v_{\text{rel}}$ and $s = 4m_\chi^2$ up to corrections of order $\Delta m/m_\chi$ and v_{rel}^2 we obtain

$$\sigma v_{\text{rel}} = \frac{v'_{\text{rel}}}{64\pi m_\chi^2} \frac{4g^4 m_\chi^4}{(N-1)} \frac{1}{t_0 - t_1} \int_{t_1}^{t_0} dt \frac{1}{(t - m_{A^\pm}^2)^2} = \frac{g^4 m_\chi^2 v'_{\text{rel}}}{16\pi(N-1)} \frac{1}{(t_0 - m_{A^\pm}^2)(t_1 - m_{A^\pm}^2)}. \quad (\text{D5})$$

Inserting $t_{0,1}$ and using (D3) we obtain

$$\sigma_{v_{\text{rel}}} = \frac{\pi\alpha_d^2}{N-1} \frac{m_\chi^2}{(m_{A^\pm}^2 + 2m_\chi\Delta m)^2 + m_\chi^2 m_{A^\pm}^2 v_{\text{rel}}^2} \sqrt{v_{\text{rel}}^2 + \frac{8\Delta m}{m_\chi}}. \quad (\text{D6})$$

We are mostly interested in the conversion cross section when the temperature drops somewhat below the mass splitting, i.e. $T_d \sim m_\chi v_{\text{rel}}^2 \lesssim \Delta m$. In this case we can estimate the cross section by its zero-velocity limit

$$\sigma_{v_{\text{rel}}|v_{\text{rel}} \rightarrow 0} = \frac{\pi\alpha_d^2}{N-1} \frac{m_\chi^2}{(m_{A^\pm}^2 + 2m_\chi\Delta m)^2} \sqrt{\frac{8\Delta m}{m_\chi}}. \quad (\text{D7})$$

Appendix E: Non-Abelian gauge boson interactions

The generators t^A of $SU(N)$ can be split into three categories as given in (B4). Here we are interested in the self-interaction of gauge bosons after symmetry breaking. We consider only triple gauge boson interactions, which are sufficient for our purposes. We start from the full $SU(N)$ case where the triple gauge boson interaction of $A_\mu^A(k), A_\nu^B(q), A_\rho^C(p)$ with all incoming momenta is given by the Feynman rule

$$gf^{ABC}(g^{\mu\nu}(k-q)^\rho + g^{\nu\rho}(q-p)^\mu + g^{\rho\mu}(p-k)^\nu). \quad (\text{E1})$$

The interaction is completely determined by the structure constants f^{ABC} of $SU(N)$, defined via

$$[t^A, t^B] = if^{ABC}t^C. \quad (\text{E2})$$

We can use the generators from (B4). We denote by $a, b, c = 1, \dots, (N-1)^2 - 1$ the indices belonging to the generators of the unbroken $SU(N-1)$ subgroup. They satisfy the corresponding commutation relations, with structure constants f^{abc} from $SU(N-1)$. Thus, as expected, the massless gauge bosons feature usual non-Abelian gauge interactions as dictated by the residual $SU(N-1)$ gauge symmetry.

Next consider the off-diagonal generators with respect to the $N-1$ subspace and the N -component of the broken color direction. They are given in (B4). We denote those involving \mathbf{e}_j or $i\mathbf{e}_j$ by t^{ej} or t^{ie_j} , respectively, for $j = 1, \dots, N-1$. It is convenient to define $t^{j\pm} \equiv \frac{1}{\sqrt{2}}(t^{ej} \mp it^{ie_j})$.

Finally, the last generator in (B4) is denoted by t^0 . Using the gauge boson notation from Sec. B 1 we have

$$A_\mu^A t^A = A_\mu^a t^a + A_\mu^{j+} t^{j+} + A_\mu^{j-} t^{j-} + A_\mu^0 t^0. \quad (\text{E3})$$

Using this basis we find that only the following structure constants (plus the ones obtained from arbitrary permutations of the indices) are in general non-zero

$$\begin{aligned} f^{abc} & , \\ f^{j\pm 0j\pm} & = \frac{\pm iN}{\sqrt{2N(N-1)}}, \\ f^{j\pm ai\pm} & = \pm i t_{ij}^a. \end{aligned} \quad (\text{E4})$$

Note that in the \pm basis, the structure constants are complex (the $\pm i$ prefactors), which is related to the property that $(t^{j+})^\dagger = t^{j-}$.

-
- [1] A. G. Riess *et al.*, A Comprehensive Measurement of the Local Value of the Hubble Constant with $1 \text{ km s}^{-1} \text{ Mpc}^{-1}$ Uncertainty from the Hubble Space Telescope and the SH0ES Team, *Astrophys. J. Lett.* **934**, L7 (2022), arXiv:2112.04510 [astro-ph.CO].
 - [2] L. Breuval, A. G. Riess, S. Casertano, W. Yuan, L. M. Macri, M. Romaniello, Y. S. Murakami, D. Scolnic, G. S. Anand, and I. Soszyński, Small magellanic cloud cepheids observed with the hubble space telescope provide a new anchor for the sh0es distance ladder, *The Astrophysical Journal* **973**, 30 (2024).
 - [3] C. Vogl *et al.*, No rungs attached: A distance-ladder free determination of the Hubble constant through type II supernova spectral modelling (2024), arXiv:2411.04968 [astro-ph.CO].
 - [4] D. Scolnic, A. G. Riess, J. Wu, S. Li, G. S. Anand, R. Beaton, S. Casertano, R. I. Anderson, S. Dhawan, and X. Ke, CATS: The Hubble Constant from Standardized TRGB and Type Ia Supernova Measurements, *Astrophys. J. Lett.* **954**, L31 (2023), arXiv:2304.06693 [astro-ph.CO].
 - [5] W. L. Freedman, B. F. Madore, T. J. Hoyt, I. S. Jang, A. J. Lee, and K. A. Owens, Status Report on the Chicago-Carnegie Hubble Program (CCHP): Measurement of the Hubble Constant Using the Hubble and James Webb Space Telescopes, *Astrophys. J.* **985**, 203 (2025), arXiv:2408.06153 [astro-ph.CO].
 - [6] T. Collaboration, S. Birrer, E. J. Buckley-Geer, M. Cappellari, F. Courbin, F. Dux, C. D. Fassnacht, J. A. Frieman, A. Galan, D. Gilman, X.-Y. Huang, S. Knabel, D. Langeroodi, H. Lin, M. Millon, T. Morishita, V. Motta, P. Mozumdar, E. Paic, A. J. Shajib, W. Sheu, D. Sluse, A. Sonnenfeld, C. Spiniello, M. Stiavelli, S. H. Suyu, C. Y. Tan, T. Treu, L. V. de Vyvere, H. Wang, P. Wells, D. M. Williams, and K. C. Wong, Tdcosmo 2025: Cosmological constraints from strong lensing time delays (2025), arXiv:2506.03023 [astro-ph.CO].
 - [7] J. P. Blakeslee, J. B. Jensen, C.-P. Ma, P. A. Milne, and J. E. Greene, The Hubble Constant from Infrared Surface Brightness Fluctuation Distances, *Astrophys. J.* **911**, 65 (2021), arXiv:2101.02221 [astro-ph.CO].
 - [8] N. Aghanim *et al.* (Planck), Planck 2018 results. VI. Cosmological parameters, *Astron. Astrophys.* **641**, A6 (2020), [Erratum: *Astron. Astrophys.* 652, C4 (2021)], arXiv:1807.06209 [astro-ph.CO].
 - [9] E. Di Valentino *et al.* (CosmoVerse), The CosmoVerse White Paper: Addressing observational tensions in cosmology with systematics and fundamental physics, *Physics of the Dark Universe*, 101965 (2025), arXiv:2504.01669 [astro-ph.CO].
 - [10] E. Camphuis *et al.* (SPT-3G), SPT-3G D1: CMB temperature and polarization power spectra and cosmology from 2019 and 2020 observations of the SPT-3G Main field (2025), arXiv:2506.20707 [astro-ph.CO].
 - [11] E. Calabrese *et al.* (ACT), The Atacama Cosmology Telescope: DR6 Constraints on Extended Cosmological Models (2025), arXiv:2503.14454 [astro-ph.CO].
 - [12] M. Abdul Karim *et al.* (DESI), DESI DR2 Results II: Measurements of Baryon Acoustic Oscillations and Cosmological Constraints (2025), arXiv:2503.14738 [astro-ph.CO].
 - [13] L. Knox and M. Millea, Hubble constant hunter’s guide, *Phys. Rev. D* **101**, 043533 (2020), arXiv:1908.03663 [astro-ph.CO].
 - [14] G. Benevento, W. Hu, and M. Raveri, Can Late Dark Energy Transitions Raise the Hubble constant?, *Phys. Rev. D* **101**, 103517 (2020), arXiv:2002.11707 [astro-ph.CO].
 - [15] F. Niedermann and M. S. Sloth, New early dark energy, *Phys. Rev. D* **103**, L041303 (2021), arXiv:1910.10739 [astro-ph.CO].
 - [16] F. Niedermann and M. S. Sloth, Resolving the Hubble tension with new early dark energy, *Phys. Rev. D* **102**, 063527 (2020), arXiv:2006.06686 [astro-ph.CO].
 - [17] F. Niedermann and M. S. Sloth, Hot new early dark energy: Towards a unified dark sector of neutrinos, dark energy and dark matter, *Phys. Lett. B* **835**, 137555 (2022), arXiv:2112.00759 [hep-ph].
 - [18] F. Niedermann and M. S. Sloth, Hot new early dark energy, *Phys. Rev. D* **105**, 063509 (2022), arXiv:2112.00770 [hep-ph].
 - [19] J. S. Cruz, F. Niedermann, and M. S. Sloth, Cold New Early Dark Energy pulls the trigger on the H_0 and S_8 tensions: a simultaneous solution to both tensions without new ingredients, *JCAP* **11**, 033, arXiv:2305.08895 [astro-ph.CO].
 - [20] M. Garny, F. Niedermann, H. Rubira, and M. S. Sloth, Hot new early dark energy bridging cosmic gaps: Supercooled phase transition reconciles stepped dark radiation solutions to the Hubble tension with BBN, *Phys. Rev. D* **110**, 023531 (2024), arXiv:2404.07256 [astro-ph.CO].
 - [21] F. Niedermann and M. S. Sloth, New Early Dark Energy as a solution to the H_0 and S_8 tensions, in *The Hubble constant tension*, edited by E. di Valentino and D. Brout (Springer, Singapore, 2024) arXiv:2307.03481 [hep-ph].
 - [22] N. Schöneberg, G. Franco Abellán, A. Pérez Sánchez, S. J. Witte, V. Poulin, and J. Lesgourgues, The H_0 Olympics: A fair ranking of proposed models, *Phys. Rept.* **984**, 1 (2022), arXiv:2107.10291 [astro-ph.CO].
 - [23] K. Freese and M. W. Winkler, Chain early dark energy: A Proposal for solving the Hubble tension and explaining today’s dark energy, *Phys. Rev. D* **104**, 083533 (2021), arXiv:2102.13655 [astro-ph.CO].
 - [24] I. J. Allali, M. P. Hertzberg, and F. Rompineve, Dark sector to restore cosmological concordance, *Phys. Rev. D* **104**, L081303 (2021), arXiv:2104.12798 [astro-ph.CO].
 - [25] E. I. Guendelman, R. Herrera, and P. Labrana, Connecting Early Dark Energy to Late Dark Energy by the Diluting Matter Potential (2025), arXiv:2507.17095 [gr-qc].
 - [26] V. Poulin, T. L. Smith, T. Karwal, and M. Kamionkowski, Early Dark Energy Can Resolve The Hubble Tension, *Phys. Rev. Lett.* **122**, 221301 (2019), arXiv:1811.04083 [astro-ph.CO].
 - [27] V. Poulin, T. L. Smith, and T. Karwal, The Ups and Downs of Early Dark Energy solutions to the Hubble tension: A review of models, hints and constraints circa 2023, *Phys. Dark Univ.* **42**, 101348 (2023), arXiv:2302.09032 [astro-ph.CO].

- [28] N. Kaloper, Dark energy, H_0 and weak gravity conjecture, *Int. J. Mod. Phys. D* **28**, 1944017 (2019), arXiv:1903.11676 [hep-th].
- [29] M. A. Buen-Abad, G. Marques-Tavares, and M. Schmaltz, Non-Abelian dark matter and dark radiation, *Phys. Rev. D* **92**, 023531 (2015), arXiv:1505.03542 [hep-ph].
- [30] M. A. Buen-Abad, M. Schmaltz, J. Lesgourgues, and T. Brinckmann, Interacting Dark Sector and Precision Cosmology, *JCAP* **01**, 008, arXiv:1708.09406 [astro-ph.CO].
- [31] M. Archidiacono, S. Gariazzo, C. Giunti, S. Hannestad, and T. Tram, Sterile neutrino self-interactions: H_0 tension and short-baseline anomalies, *JCAP* **12**, 029, arXiv:2006.12885 [astro-ph.CO].
- [32] N. Blinov and G. Marques-Tavares, Interacting radiation after Planck and its implications for the Hubble Tension, *JCAP* **09**, 029, arXiv:2003.08387 [astro-ph.CO].
- [33] D. Aloni, A. Berlin, M. Joseph, M. Schmaltz, and N. Weiner, A Step in understanding the Hubble tension, *Phys. Rev. D* **105**, 123516 (2022), arXiv:2111.00014 [astro-ph.CO].
- [34] E. Witten, Cosmological Consequences of a Light Higgs Boson, *Nucl. Phys. B* **177**, 477 (1981).
- [35] S. R. Coleman and E. J. Weinberg, Radiative Corrections as the Origin of Spontaneous Symmetry Breaking, *Phys. Rev. D* **7**, 1888 (1973).
- [36] J. Lesgourgues, G. Marques-Tavares, and M. Schmaltz, Evidence for dark matter interactions in cosmological precision data?, *JCAP* **02**, 037, arXiv:1507.04351 [astro-ph.CO].
- [37] H. Rubira, A. Mazoun, and M. Garny, Full-shape BOSS constraints on dark matter interacting with dark radiation and lifting the S_8 tension, *JCAP* **01**, 034, arXiv:2209.03974 [astro-ph.CO].
- [38] L. G. van den Aarssen, T. Bringmann, and C. Pfrommer, Is dark matter with long-range interactions a solution to all small-scale problems of Λ CDM cosmology?, *Phys. Rev. Lett.* **109**, 231301 (2012), arXiv:1205.5809 [astro-ph.CO].
- [39] F.-Y. Cyr-Racine, K. Sigurdson, J. Zavala, T. Bringmann, M. Vogelsberger, and C. Pfrommer, ETHOS—an effective theory of structure formation: From dark particle physics to the matter distribution of the Universe, *Phys. Rev. D* **93**, 123527 (2016), arXiv:1512.05344 [astro-ph.CO].
- [40] Z. Chacko, Y. Cui, S. Hong, T. Okui, and Y. Tsai, Partially Acoustic Dark Matter, Interacting Dark Radiation, and Large Scale Structure, *JHEP* **12**, 108, arXiv:1609.03569 [astro-ph.CO].
- [41] T. Binder, L. Covi, A. Kamada, H. Murayama, T. Takahashi, and N. Yoshida, Matter Power Spectrum in Hidden Neutrino Interacting Dark Matter Models: A Closer Look at the Collision Term, *JCAP* **11**, 043, arXiv:1602.07624 [hep-ph].
- [42] M. Ibe, S. Matsumoto, and R. Sato, Mass Splitting between Charged and Neutral Winos at Two-Loop Level, *Phys. Lett. B* **721**, 252 (2013), arXiv:1212.5989 [hep-ph].
- [43] D. Blas, J. Lesgourgues, and T. Tram, The Cosmic Linear Anisotropy Solving System (CLASS) II: Approximation schemes, *JCAP* **07**, 034, arXiv:1104.2933 [astro-ph.CO].
- [44] D. Brout *et al.*, The Pantheon+ Analysis: Cosmological Constraints, *Astrophys. J.* **938**, 110 (2022), arXiv:2202.04077 [astro-ph.CO].
- [45] L. Herold, E. G. M. Ferreira, and E. Komatsu, New Constraint on Early Dark Energy from Planck and BOSS Data Using the Profile Likelihood, *Astrophys. J. Lett.* **929**, L16 (2022), arXiv:2112.12140 [astro-ph.CO].
- [46] J. S. Cruz, S. Hannestad, E. B. Holm, F. Niedermann, M. S. Sloth, and T. Tram, Profiling cold new early dark energy, *Phys. Rev. D* **108**, 023518 (2023), arXiv:2302.07934 [astro-ph.CO].
- [47] D. E. Kaplan, G. Z. Krnjaic, K. R. Rehermann, and C. M. Wells, Atomic Dark Matter, *JCAP* **05**, 021, arXiv:0909.0753 [hep-ph].
- [48] F.-Y. Cyr-Racine and K. Sigurdson, Cosmology of atomic dark matter, *Phys. Rev. D* **87**, 103515 (2013), arXiv:1209.5752 [astro-ph.CO].
- [49] F.-Y. Cyr-Racine, F. Ge, and L. Knox, Symmetry of Cosmological Observables, a Mirror World Dark Sector, and the Hubble Constant, *Phys. Rev. Lett.* **128**, 201301 (2022), arXiv:2107.13000 [astro-ph.CO].
- [50] N. Blinov, G. Krnjaic, and S. W. Li, Toward a realistic model of dark atoms to resolve the Hubble tension, *Phys. Rev. D* **105**, 095005 (2022), arXiv:2108.11386 [hep-ph].
- [51] S. Bansal, J. Barron, D. Curtin, and Y. Tsai, Precision cosmological constraints on atomic dark matter, *JHEP* **10**, 095, arXiv:2212.02487 [hep-ph].
- [52] M. Joseph, D. Aloni, M. Schmaltz, E. N. Sivarajan, and N. Weiner, A Step in understanding the S_8 tension, *Phys. Rev. D* **108**, 023520 (2023), arXiv:2207.03500 [astro-ph.CO].
- [53] N. Schöneberg, G. Franco Abellán, T. Simon, A. Bartlett, Y. Patel, and T. L. Smith, Comparative analysis of interacting stepped dark radiation, *Phys. Rev. D* **108**, 123513 (2023), arXiv:2306.12469 [astro-ph.CO].
- [54] M. Vogelsberger, J. Zavala, F.-Y. Cyr-Racine, C. Pfrommer, T. Bringmann, and K. Sigurdson, ETHOS – an effective theory of structure formation: dark matter physics as a possible explanation of the small-scale CDM problems, *Mon. Not. Roy. Astron. Soc.* **460**, 1399 (2016), arXiv:1512.05349 [astro-ph.CO].
- [55] D. C. Hooper, N. Schöneberg, R. Murgia, M. Archidiacono, J. Lesgourgues, and M. Viel, One likelihood to bind them all: Lyman- α constraints on non-standard dark matter, *JCAP* **10**, 032, arXiv:2206.08188 [astro-ph.CO].
- [56] M. A. Buen-Abad, Z. Chacko, C. Kilic, G. Marques-Tavares, and T. Youn, Stepped partially acoustic dark matter: likelihood analysis and cosmological tensions, *JCAP* **11**, 005, arXiv:2306.01844 [astro-ph.CO].
- [57] A. Mazoun, S. Bocquet, M. Garny, J. J. Mohr, H. Rubira, and S. M. L. Vogt, Probing interacting dark sector models with future weak lensing-informed galaxy cluster abundance constraints from SPT-3G and CMB-S4, *Phys. Rev. D* **109**, 063536 (2024), arXiv:2312.17622 [astro-ph.CO].
- [58] A. Mazoun *et al.* (SPT, DES), Interacting dark sector within ETHOS: Cosmological constraints from SPT cluster abundance with DES and HST weak lensing data, *Phys. Rev. D* **111**, 083543 (2025), arXiv:2411.19911 [astro-ph.CO].

- [59] J. Lesgourgues *et al.* (Euclid), Euclid preparation - LVI. Sensitivity to non-standard particle dark matter models, *Astron. Astrophys.* **693**, A249 (2025), arXiv:2406.18274 [astro-ph.CO].
- [60] L. J. Hall, K. Jedamzik, J. March-Russell, and S. M. West, Freeze-In Production of FIMP Dark Matter, *JHEP* **03**, 080, arXiv:0911.1120 [hep-ph].
- [61] M. Garny, M. Sandora, and M. S. Sloth, Planckian Interacting Massive Particles as Dark Matter, *Phys. Rev. Lett.* **116**, 101302 (2016), arXiv:1511.03278 [hep-ph].
- [62] M. Garny, A. Palessandro, M. Sandora, and M. S. Sloth, Charged Planckian Interacting Dark Matter, *JCAP* **01**, 021, arXiv:1810.01428 [hep-ph].
- [63] J. Harz and K. Petraki, Radiative bound-state formation in unbroken perturbative non-Abelian theories and implications for dark matter, *JHEP* **07**, 096, arXiv:1805.01200 [hep-ph].
- [64] T. Binder, K. Mukaida, B. Scheihing-Hitschfeld, and X. Yao, Non-Abelian electric field correlator at NLO for dark matter relic abundance and quarkonium transport, *JHEP* **01**, 137, arXiv:2107.03945 [hep-ph].
- [65] T. Binder, M. Garny, J. Heisig, S. Lederer, and K. Urban, Excited bound states and their role in dark matter production, *Phys. Rev. D* **108**, 095030 (2023), arXiv:2308.01336 [hep-ph].
- [66] G. F. Giudice, H. M. Lee, A. Pomarol, and B. Shakya, Nonthermal heavy dark matter from a first-order phase transition, *JHEP* **12**, 190, arXiv:2403.03252 [hep-ph].
- [67] G. D. Moore and D. Teaney, How much do heavy quarks thermalize in a heavy ion collision?, *Phys. Rev. C* **71**, 064904 (2005), arXiv:hep-ph/0412346.
- [68] S. J. Huber and T. Konstandin, Gravitational Wave Production by Collisions: More Bubbles, *JCAP* **09**, 022, arXiv:0806.1828 [hep-ph].
- [69] C. Caprini, R. Durrer, and G. Servant, Gravitational wave generation from bubble collisions in first-order phase transitions: An analytic approach, *Phys. Rev. D* **77**, 124015 (2008), arXiv:0711.2593 [astro-ph].
- [70] R. Jinno and M. Takimoto, Gravitational waves from bubble collisions: An analytic derivation, *Phys. Rev. D* **95**, 024009 (2017), arXiv:1605.01403 [astro-ph.CO].
- [71] M. Hindmarsh, S. J. Huber, K. Rummukainen, and D. J. Weir, Gravitational waves from the sound of a first order phase transition, *Phys. Rev. Lett.* **112**, 041301 (2014), arXiv:1304.2433 [hep-ph].
- [72] M. Hindmarsh, S. J. Huber, K. Rummukainen, and D. J. Weir, Numerical simulations of acoustically generated gravitational waves at a first order phase transition, *Phys. Rev. D* **92**, 123009 (2015), arXiv:1504.03291 [astro-ph.CO].
- [73] R. Jinno, T. Konstandin, H. Rubira, and I. Stomberg, Higgsless simulations of cosmological phase transitions and gravitational waves, *JCAP* **02**, 011, arXiv:2209.04369 [astro-ph.CO].
- [74] C. Caprini, R. Jinno, T. Konstandin, A. R. Pol, H. Rubira, and I. Stomberg, Gravitational waves from first-order phase transitions: from weak to strong, *Journal of High Energy Physics* **2025**, 10.1007/jhep07(2025)217 (2025).
- [75] J. Antoniadis *et al.* (EPTA, InPTA:), The second data release from the European Pulsar Timing Array - III. Search for gravitational wave signals, *Astron. Astrophys.* **678**, A50 (2023), arXiv:2306.16214 [astro-ph.HE].
- [76] G. Agazie *et al.* (NANOGrav), The NANOGrav 15 yr Data Set: Evidence for a Gravitational-wave Background, *Astrophys. J. Lett.* **951**, L8 (2023), arXiv:2306.16213 [astro-ph.HE].
- [77] G. Elor, R. Jinno, S. Kumar, R. McGehee, and Y. Tsai, Finite bubble statistics constrain late cosmological phase transitions (2023), arXiv:2311.16222 [hep-ph].
- [78] D. Aloni, M. Joseph, M. Schmaltz, and N. Weiner, Dark Radiation from Neutrino Mixing after Big Bang Nucleosynthesis, *Phys. Rev. Lett.* **131**, 221001 (2023), arXiv:2301.10792 [astro-ph.CO].
- [79] R. Z. Ferreira, A. Notari, O. Pujolas, and F. Rompineve, Gravitational waves from domain walls in Pulsar Timing Array datasets, *JCAP* **02**, 001, arXiv:2204.04228 [astro-ph.CO].
- [80] K. Ichikawa, M. Kawasaki, K. Nakayama, M. Senami, and F. Takahashi, Increasing effective number of neutrinos by decaying particles, *JCAP* **05**, 008, arXiv:hep-ph/0703034.
- [81] W. Fischler and J. Meyers, Dark Radiation Emerging After Big Bang Nucleosynthesis?, *Phys. Rev. D* **83**, 063520 (2011), arXiv:1011.3501 [astro-ph.CO].
- [82] A. C. Sobotka, A. L. Erickcek, and T. L. Smith, Comprehensive constraints on dark radiation injection after BBN, *Phys. Rev. D* **109**, 063538 (2024), arXiv:2312.13235 [astro-ph.CO].
- [83] N. Schöneberg and G. Franco Abellán, A step in the right direction? Analyzing the Wess Zumino Dark Radiation solution to the Hubble tension, *JCAP* **12**, 001, arXiv:2206.11276 [astro-ph.CO].
- [84] C.-P. Ma and E. Bertschinger, Cosmological perturbation theory in the synchronous and conformal Newtonian gauges, *Astrophys. J.* **455**, 7 (1995), arXiv:astro-ph/9506072.
- [85] M.-X. Lin, G. Benevento, W. Hu, and M. Raveri, Acoustic Dark Energy: Potential Conversion of the Hubble Tension, *Phys. Rev. D* **100**, 063542 (2019), arXiv:1905.12618 [astro-ph.CO].
- [86] N. Aghanim *et al.* (Planck), Planck 2018 results. VIII. Gravitational lensing, *Astron. Astrophys.* **641**, A8 (2020), arXiv:1807.06210 [astro-ph.CO].
- [87] B. Audren, J. Lesgourgues, K. Benabed, and S. Prunet, Conservative Constraints on Early Cosmology: an illustration of the Monte Python cosmological parameter inference code, *JCAP* **1302**, 001, arXiv:1210.7183 [astro-ph.CO].
- [88] T. Brinckmann and J. Lesgourgues, Montepython 3: boosted mcmc sampler and other features (2018), arXiv:1804.07261 [astro-ph.CO].
- [89] A. Lewis, GetDist: a Python package for analysing Monte Carlo samples (2019), arXiv:1910.13970 [astro-ph.IM].
- [90] A. Gelman and D. B. Rubin, Inference from Iterative Simulation Using Multiple Sequences, *Statist. Sci.* **7**, 457 (1992).
- [91] M. Raveri and W. Hu, Concordance and Discordance in Cosmology, *Phys. Rev. D* **99**, 043506 (2019), arXiv:1806.04649 [astro-ph.CO].

- [92] T. Karwal, Y. Patel, A. Bartlett, V. Poulin, T. L. Smith, and D. N. Pfeffer, Procoli: Profiles of cosmological likelihoods (2024), arXiv:2401.14225 [astro-ph.CO].
- [93] I. J. Allali, F. Rompineve, and M. P. Hertzberg, Dark sectors with mass thresholds face cosmological datasets, Phys. Rev. D **108**, 023527 (2023), arXiv:2305.14166 [astro-ph.CO].
- [94] A. R. Khalife, M. B. Zanjani, S. Galli, S. Günther, J. Lesgourgues, and K. Benabed, Review of Hubble tension solutions with new SH0ES and SPT-3G data, JCAP **04**, 059, arXiv:2312.09814 [astro-ph.CO].
- [95] A. Vasudevan, M. M. Ivanov, S. Sibiryakov, and J. Lesgourgues, Time-sliced perturbation theory with primordial non-Gaussianity and effects of large bulk flows on inflationary oscillating features, JCAP **09**, 037, arXiv:1906.08697 [astro-ph.CO].
- [96] T. Mergulhão, F. Beutler, and J. A. Peacock, Primordial feature constraints from BOSS + eBOSS, JCAP **08**, 012, arXiv:2303.13946 [astro-ph.CO].
- [97] D. Green, Y. Guo, J. Han, and B. Wallisch, Light fields during inflation from BOSS and future galaxy surveys, JCAP **05**, 090, arXiv:2311.04882 [astro-ph.CO].
- [98] M. Ballardini and N. Barbieri, Refining the nonlinear modelling of primordial oscillatory features, JCAP **05**, 059, arXiv:2411.02261 [astro-ph.CO].
- [99] T. Louis *et al.* (ACT), The Atacama Cosmology Telescope: DR6 Power Spectra, Likelihoods and Λ CDM Parameters (2025), arXiv:2503.14452 [astro-ph.CO].
- [100] V. Poulin, T. L. Smith, R. Calderón, and T. Simon, Impact of ACT DR6 and DESI DR2 for Early Dark Energy and the Hubble tension (2025), arXiv:2505.08051 [astro-ph.CO].
- [101] A. R. Khalife *et al.*, SPT-3G D1: Axion Early Dark Energy with CMB experiments and DESI (2025), arXiv:2507.23355 [astro-ph.CO].
- [102] M. Cicoli, M. Licheri, R. Mahanta, E. McDonough, F. G. Pedro, and M. Scalisi, Early Dark Energy in Type IIB String Theory, JHEP **06**, 052, arXiv:2303.03414 [hep-th].